CHEMICAL REVIEWS

Subscriber access provided by V. Vernadsky | National Library of Ukraine

Microcantilevers: Sensing Chemical Interactions via Mechanical Motion

Karen M. Goeders, Jonathan S. Colton, and Lawrence A. Bottomley

Chem. Rev., **2008**, 108 (2), 522-542 • DOI: 10.1021/cr0681041

Downloaded from http://pubs.acs.org on December 24, 2008

More About This Article

Additional resources and features associated with this article are available within the HTML version:

- Supporting Information
- Links to the 3 articles that cite this article, as of the time of this article download
- Access to high resolution figures
- Links to articles and content related to this article
- Copyright permission to reproduce figures and/or text from this article

View the Full Text HTML

ACS Publications
High quality. High impact.

Chemical Reviews is published by the American Chemical Society. 1155 Sixteenth Street N.W., Washington, DC 20036

Microcantilevers: Sensing Chemical Interactions via Mechanical Motion

Karen M. Goeders,† Jonathan S. Colton,‡ and Lawrence A. Bottomley*,†

School of Chemistry & Biochemistry and George W. Woodruff School of Mechanical Engineering, Georgia Institute of Technology, Atlanta, Georgia 30332

Received September 21, 2007

Contents

1. Introduction 522
2. Theory of Operation 522
2.1. Static Deflection 523
2.2. Dynamic Response 525
2.2.1. Mass–Spring–Dashpot System. 525
2.2.2. Quality Factor 525
2.2.3. Plane Strain 525
2.2.4. Bending Mode Frequency Response 526
2.2.5. Effect of Damping Due to Viscous Fluids 526
2.2.6. Effect of Air Damping on Quality Factor 527
2.3. Lateral and Torsional Mode Frequency Responses 527
2.4. Temperature Effects 527
2.4.1. Effect on Material Properties 528
2.4.2. Effect on Geometry 528
3. Detection Schemes 528
3.1. Optical Lever 528
3.2. Interferometer 529
3.3. Piezoresistive 529
3.4. Capacitive 529
4. Design, Materials, and Fabrication 529
4.1. Design Considerations 530
4.2. Fabrication of Silicon-based Cantilevers 530
4.2.1. Film Deposition 530
4.2.2. Photolithography 530
4.2.3. Etching 530
4.2.4. Doping 530
4.3. Fabrication of Polymeric Cantilevers 531
5. Chemical Selectivity 531
6. Chemical Applications 533
6.1. Volatile Organics 533
6.2. Chemical Warfare Agents 534
6.3. Explosives 534
6.4. Toxic Metal Ions 534
7. Biological Applications 534
7.1. Cells 534
7.2. Viruses 534
7.3. Antigen–Antibody Interactions 535
7.4. DNA Hybridization 536
7.5. Enzymes 537
8. Recommendations for Future Work 538
8.1. Guidelines for Reporting Sensor Performance 538
8.2. Experimental Design Considerations 538
8.3. Fruitful Areas for Further Research 539
8.3.1. More Selective Coatings 539
8.3.2. Increased Sensitivity and Faster Response 539
9. References 539

1. Introduction

Micromechanical devices comprise emerging sensor platforms with straightforward sensing mechanisms. Molecular adsorption onto the sensing element, typically a cantilever, shifts its resonance frequency and changes its surface forces (surface stress). Adsorption onto the sensing element composed of two chemically different surfaces produces a differential stress between the two surfaces and induces bending. The analyte that induces the mechanical response may be physi- or chemisorbed onto the cantilever in a reversible or irreversible process. Devices that respond to chemical stimuli in this manner are more commonly referred to as microcantilever sensors.[1−6] A compelling feature of microcantilever sensors is that they can be operated in air, vacuum, or liquid. The rapid growth in microcantilever-based sensor technology parallels advancements in micromachining methodologies and is in response to the need for more sensitive and selective detection of airborne and waterborne toxic and pathogenic substances.

The purpose of this review is to critically examine the current state of theory, modes of detection, design considerations, and innovative applications of this sensing platform. Each will be addressed separately in the following sections. At the conclusion of this review, we will identify areas that warrant further investigation and suggest guidelines for reporting the performance of microcantilever sensors to facilitate comparison of microcantilevers with other sensing platforms.

2. Theory of Operation

Microcantilever sensors rely on their deflection to indicate sensing. This section describes the theory for the mechanical response of microcantilevers in the bending, lateral, and torsional modes when used as sensors. This discussion is divided into the two modes of microcantilever deflection, static and dynamic, that are used in sensing applications. The means for detecting deflection are discussed in a separate section.

The static mode of deflection occurs when an adsorbed species causes differential surface stresses on the oppo-

* To whom correspondence should be addressed. E-mail: lawrence.bottomley@chemistry.gatech.edu.
† School of Chemistry & Biochemistry.
‡ George W. Woodruff School of Mechanical Engineering.

10.1021/cr0681041 CCC: $71.00 © 2008 American Chemical Society
Published on Web 01/30/2008

Karen Meloy Goeders is pursuing her doctorate in analytical chemistry from the Georgia Institute of Technology. She came to the School of Chemistry & Biochemistry after completing her B.S. degree in chemistry from Louisiana State University. Her dissertation research focuses on developing microcantilever array technology for enzymatic assays.

Dr. Jonathan Colton is a professor of mechanical engineering at the Georgia Institute of Technology. He obtained his S.B., S.M., and Ph.D. in Mechanical Engineering at the Massachusetts Institute of Technology. He serves as the director of the Center for Polymer Processing. He is a fellow of the American Society of Mechanical Engineers and of the Society of Plastics Engineers and is a registered professional engineer in the state of Georgia. His research interests include polymer and polymer composites processing, bioMEMS sensors, biomedical devices, and dielectric materials.

Dr. Lawrence A. Bottomley is a professor of chemistry at the Georgia Institute of Technology. He obtained his B.S. in chemistry at California State University, Fullerton, and his Ph.D. in analytical chemistry at the University of Houston. His current research interests include the biological and nanotechnological applications of scanning probe microscopy, electroanalytical chemistry, and microcantilever array sensing.

site surfaces of the microcantilever. The equations that describe the static deflection of microcantilevers will be presented, and the response of the deflection to surface stress will be discussed. In the dynamic mode of detection, the frequency of vibration of the beam changes as species are adsorbed onto the microcantilever. The equations describing the vibration of the beam in air will be presented. The damping effects of measurement in a viscous gas and liquid will be described next. Thermal effects also will be discussed.

A microcantilever can be modeled as a cantilever beam (thickness, t; width, w; and length, L), which is built in (fixed) at one of its ends (see Figure 1).[7] Note that, in Figure 1, z denotes the deflection in the thickness direction along the beam length and time [i.e., $z(x,T)$] and does not indicate the origin of the coordinate system. The discussion first will be limited to pure bending of a beam; lateral and torsional (twisting) motions will be discussed at the end of this section. Figure 2 shows the bending (a), lateral (b), and torsional (c) deflections of a built-in beam.[7]

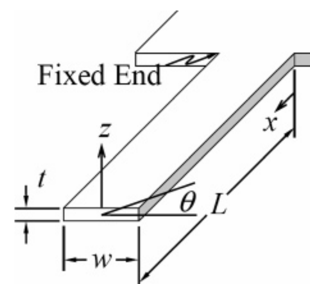

Figure 1. Microcantilever geometry and nomenclature.

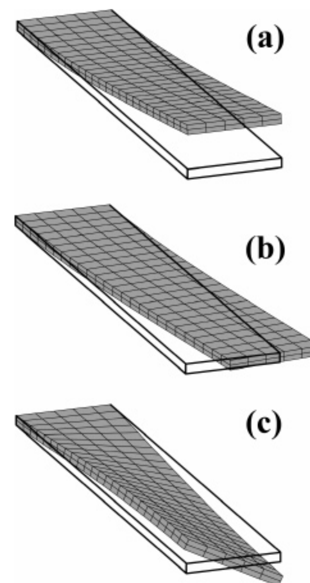

Figure 2. Schematic of the first bending (a), lateral (b), and torsional (c) modes of a resonating cantilever. The heavy lines denote the undeformed cantilever; the shaded regions denote the deformed cantilever.

2.1. Static Deflection

Static deflection is used to determine the amount of material adsorbed onto a microcantilever. The more material that is adsorbed, the more the microcantilever will deflect.[8-10] Deflection results from two mechanisms: added mass and surface stress from adsorbed species.[11-13] However, the surface stress may not necessarily correlate with the amount

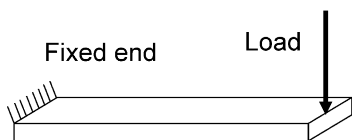

Figure 3. End-loaded beam.

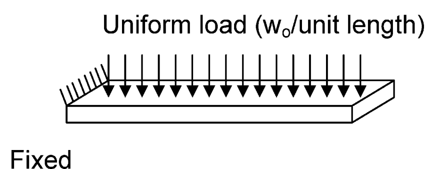

Figure 4. Beam loaded by a uniform load (w_o/unit length).

of material adsorbed. The deflection of the free end of the beam depends on the type of loading to which the beam is subjected. If a concentrated load, F, is applied to the free end of a rectangular beam (see Figure 3), then the deflection of the free end of the beam, δ, is given by eq 1[14]

$$\delta = \frac{FL^3}{3EI} \quad (1)$$

where E is the Young's elastic modulus of the beam material, L is the length of beam, and I is the second moment of the beam's cross-sectional area. I is a function of the beam width, w, and thickness, t, and is equal to $wt^3/12$. The resistance to bending deformation (i.e., stiffness) in bending of a rectangular beam (k) is given by eq 2.[15]

$$k = \frac{3EI}{L^3} \quad (2)$$

An example of this type of deflection is a tipped microcantilever used in atomic force microscopy to measure surface geometry. Equation 2 is commonly used to calculate the force constant of imaging probes. However, since the dynamic etches used to create these probes modify the shape and dimensions of both the tip and the beam, use of this equation to compute k results in significant error. Poggi et al.[16] have presented an improved method for determining beam stiffness that takes into account the actual geometry of the cantilever.

If the beam is uniformly loaded along its length by a load per unit length, w_o, (see Figure 4), the deflection of its free end is given by eq 3.[14]

$$\delta = \frac{w_o L^4}{8EI} \quad (3)$$

An example of this type of deflection is when a species is adsorbed uniformly to a cantilever's surfaces. For example, if one assumes that the species of interest absorbs only on one surface of a microcantilever, a surface stress results on that side. The difference in the stresses on the top and bottom surfaces of the cantilever generates a deflection that is independent of that due to the adsorbed mass. Stoney's equation[17] has been used to relate the difference in surface stresses on each surface of a beam to its deflection (see Figure 5)

$$\frac{1}{r} = 6\frac{Pt}{Ed^2} \quad (4)$$

where r is the radius of curvature of the beam, P is the surface stress due to a coating on one surface of the beam, t is the thickness of the coating, and d is the thickness of the beam. The radius of curvature, R, of a microcantilever under the influence of surface stresses on its top and bottom surfaces is typically reported as eq 5[18]

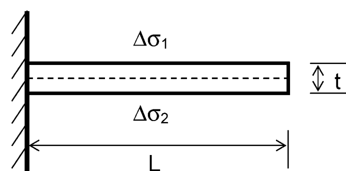

Figure 5. Fixed beam subjected to surface stresses.

$$\frac{1}{R} = 6\frac{1-\nu}{Et^2}(\Delta\sigma_1 - \Delta\sigma_2) \quad (5)$$

where υ is the Poisson's ratio of the material; it is included to reflect the plane strain condition of the microcantilever (see discussion of the Searle parameter below). $\Delta\sigma_1$ and $\Delta\sigma_2$ are the stresses that act on the top and bottom surfaces of the beam, and t is the thickness of the beam. The deflection of such a beam can be calculated using the geometric relation $R^{-1} = 2\Delta z/L^2$, where Δz is the beam's end deflection. Only a difference in absorption between the top and bottom surfaces will cause deflection; equal absorption to both top and bottom surfaces will counteract each other, resulting in no deflection. One will note that the units on the two sides of eq 5 do not match (left-hand side (LHS) = distance^{-1} vs right-hand side (RHS) = distance^{-2}); this is due to the fact that the surface stresses in Stoney's equation are reported on the basis of a per unit thickness of the layer that causes the deflection in the beam. As is convention in the literature, the term stress is used and its units are N/m. In practice, $\Delta\sigma_s = \bar{\sigma}_f t_f$, where $\bar{\sigma}_f$ is the average normal stress acting on the cross-sectional area residing in a plane that is normal to the neutral axis of the beam-coating composite and t_f is the coating thickness. Hence, $\Delta\sigma_s$ is visualized as the normal force per unit width acting on a normal section of the coating.

Stoney's equation (eqs 4 and 5) is an exact solution for plate bending that is unrestrained at all edges and assumes no interaction between adsorbed species. Hence, a more accurate equation is necessary. For a cantilever with length L (x), width w ($2y$), and thickness t (z) (see Figure 1), Sader[19] has developed a more complete solution for the deflection of a point on a fixed cantilever beam under the influence of a surface stress, $w_{cant}(X, Y)$, as shown in eq 6[20]

$$w_{cant}(X, Y) = \Omega L^2 \Bigg\{ X^2 + 2\nu X[\tau_1^{-1} + \tau_2^{-2}]\left(\frac{w}{L}\right) - [12^{-1} + 2\upsilon(\tau_1^{-2} + \tau_2^{-2} + \tau_1^{-1}\tau_2^{-1}) - \sum_{i=1}^{2} d_i(12^{-1} + 2\nu\tau_i^{-2}) \times \exp(-\tau_i XLw^{-1})]\left(\frac{w}{L}\right)^2 + Y^2[1 - \sum_{i=1}^{2} d_i \exp(-\tau_i XLw^{-1})] \Bigg\} \quad (6)$$

where $X = xL^{-1}$, $Y = yL^{-1}$, $d_i = \tau_{3-i}(\tau_{3-i} - \tau_i)^{-1}$, $\Omega = \Delta\sigma_s t/[4D(1 + \upsilon)]$, where $\Delta\sigma_s$ is the surface stress and $D = Et^3\{12(1 - \upsilon^2)\}^{-1}$ is the cantilever bending rigidity. The τ_i are defined by eq 7.

$$\tau_i = 2\sqrt{3}[5(1 - \nu + (-1)^i\sqrt{10(1 - \nu)(2 - 3\nu)})] \quad (7)$$

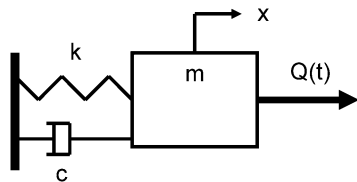

Figure 6. Mass−spring−dashpot system.

For the case where the deflection at the end of the tip is desired, $x = L$ and $y = w/2$. Klein provides an expression for the error in using Stoney's equation for a multilayer laminate.[21]

Stoney's and Sader's equations can be used to relate the deflections of microcantilevers to the surface stresses resulting from adsorbed species. Typically, the surface stress is calculated following measurement of deflection. It is difficult to determine a priori the surface stresses due to molecular attachment. In the following section on dynamic methods, we will develop expressions for the effect of surface stress on the dynamic response of a microcantilever.

2.2. Dynamic Response

In this section, the dynamic response of a simple mass−spring−dashpot system first is described to introduce the reader to the appropriate concepts. Then, the quality factor, a well-used metric of microcantilever performance, is discussed. Next, the vibration of a fixed microcantilever in air and shifts in resonant frequency resulting from added mass layers and changes in surface stress are presented. The damping effects of a liquid on vibrational frequency then are presented, which correlates to the submersion of a microcantilever in viscous gas and liquid media. Finally, the effect of temperature is discussed.

2.2.1. Mass–Spring–Dashpot System

A mass−spring−dashpot system, such as that in Figure 6, has the equation of motion shown in eq 8[21]

$$m\frac{d^2x}{dt^2} + c\frac{dx}{dt} + kx = F(t) \tag{8}$$

where m is the mass, c is the dashpot constant, k is the spring constant, and x is the displacement of the mass. $F(T)$ represents the generalized force that is exciting the system. The natural frequency of vibration (ω_{nat}) (i.e., with no excitation force, $F(t) = 0$) of the undamped beam (i.e., with no dashpot, $c = 0$) is given by eq 9.

$$\omega_{nat} = \sqrt{k/m} \tag{9}$$

When damping is present (i.e., one includes the effect of the dashpot), one can use the natural frequency to rewrite the equation of motion with no excitation force ($F(t) = 0$) as eq 10.

$$\frac{dx^2}{dt^2} + 2\zeta\omega_{nat}\frac{dx}{dt} + \omega_{nat}{}^2x = 0 \tag{10}$$

The parameter ζ is known as the system's damping and is defined for this system in eq 11.

$$\zeta = \frac{c}{2\omega_{nat}m} \equiv \frac{c}{2\sqrt{km}} \tag{11}$$

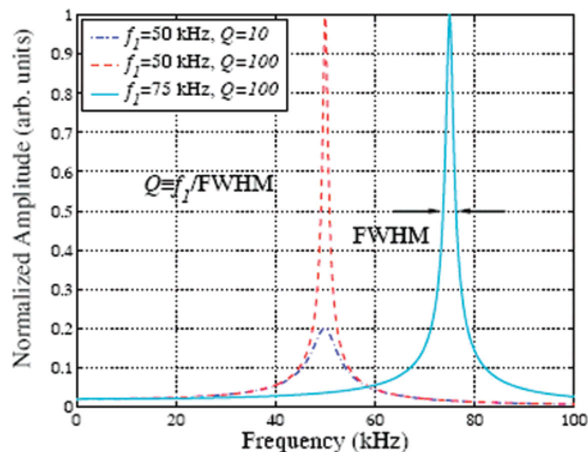

Figure 7. Generic frequency response curves.

Similarly, a freely vibrating microcantilever beam (i.e., due to thermal excitation) will resonate at its natural frequency (eq 9). Thus, as material absorbs onto the beam forming a coating, the microcantilever's vibrational frequency will decrease and, depending upon the thickness of the adsorbed layer, its spring constant may change.

2.2.2. Quality Factor

The quality factor of a microcantilever characterizes the shape of its frequency response curve (e.g., a plot of the displacement amplitude versus frequency) near a resonance mode.[22] Accordingly, each resonance mode has its own quality factor. Mathematically, the ith mode quality factor, Q_i, is defined as the ratio of the resonance frequency of the ith mode, f_i, to the full width of the resonance peak evaluated at the half-maximum (FWHM = full width half-maximum) of the peak. The quality factor indicates the narrowness of a resonant peak. Figure 7 shows generic frequency response curves and their quality factors and f_i values.[7] The definition and value of the quality factor for a lightly damped one-degree-of-freedom system, such as an AFM microcantilever, is given by eq 12[21]

$$Q_i = \frac{\omega_i}{\Delta\omega} = \frac{1}{2\zeta} = \frac{f_i}{\mathrm{FWHM}} \tag{12}$$

where $\omega_i = 2\pi f_i$ and $\Delta\omega = 2\pi$FWMH.

The quality factor depends on the cantilever geometry and the fluid in which the cantilever is immersed.[23−30] Increased damping effects lead to a lower Q value. A higher Q value is desired because it lowers the minimum detectable resonance shift (i.e., it increases the frequency resolution). For a quality factor of 10, the minimum detectable resonance frequency shift is roughly 25 Hz, whereas a quality factor of 100 allows for a frequency resolution below 10 Hz.

2.2.3. Plane Strain

The discussions in this paper assume that microcantilevers are in a plane strain situation.[18,31] The Searle parameter[32] is defined as $\beta^b = w^2\kappa_b/t$ in a bending mode (Figure 2a) and $\beta^l = t^2\kappa_l/w$ in a lateral mode (Figure 2b), where κ_b and κ_l are the principal curvatures in the bending and lateral modes, respectively, and dictate the deformational situation a beam is undergoing. A Searle parameter value < 1 indicates a plane stress situation, whereas a Searle parameter value > 100 indicates a plane strain situation.[33] From the Euler−Bernoulli beam theory,[34] the expression for the maximum curvature

of a beam subjected to a transverse deflection at its end (causing a bending or lateral deformation) of δ is $3\delta/L^2$. This implies that the maximum Searle parameter value for a bending mode is $\beta^{b}\max = 3\delta w^2/L^2 t$ and for a lateral mode is $\beta^{l}\max = 3\delta t^2/L^2 w$. Assuming an end deflection at thermal resonance of 100 nm for *both* the bending and lateral modes (the lateral mode will have a smaller deflection)[35] and using the L, w, and t values of 500, 100, and 0.8 μm, typical of silicon microcantilevers,[7,18,31] the maximum Searle parameters for the bending and lateral modes are $\beta^{b}\max = 0.015$ and $\beta^{l}\max = 7.7 \times 10^{-9}$. These are $\ll 1$, indicating a plane stress situation; hence, equations derived in this article are valid for plane strain situations.

2.2.4. Bending Mode Frequency Response

An unloaded beam freely vibrating in a bending mode (see Figure 2a) in a vacuum will have a number of resonance frequencies—frequencies at which it will naturally vibrate under thermally induced excitation. The following discussion is taken from McFarland and co-workers.[31] The general expression for the ith mode resonance of the beam, f_i, is given by eq 13

$$f_i = \frac{1}{2\pi}\left(\frac{\alpha_i}{L}\right)^2 \sqrt{\frac{EI}{\rho_b w t}} \qquad (13)$$

where ρ_b is the cantilever material density and α_i is obtained numerically from the frequency relation (eq 14).

$$\cosh \alpha_i \cos \alpha_i + 1 = 0 \qquad (14)$$

The solutions to eq 14 can be found in the report by Han and co-workers.[36]

For a rectangular beam with $I = wt^3/12$, eq 15 can be used to determine f_i

$$f_i = \frac{t}{4\pi}\left(\frac{\alpha_i}{L}\right)^2 \sqrt{\frac{EI}{3\rho_b}} \qquad (15)$$

Equation 13 can be modified further by inserting eq 2, resulting in eq 16

$$f_i = \frac{\alpha_i^2}{2\pi\sqrt{3}}\sqrt{\frac{k}{M_b}} \qquad (16)$$

where M_b is the mass of the microcantilever beam.

If a layer of molecules or other species is added to (coats) a beam, the mass of the composite beam will increase by ΔM; hence, the new resonance frequencies ($+m$) due to the mass increase will be given by eq 17. The following discussion is taken from McFarland[20] and can be used to determine the sensitivity of a microcantilever's response to added mass.

$$f_i^{+m} = \frac{\alpha_i^2}{2\pi\sqrt{3}}\sqrt{\frac{k}{M_b + \Delta M}} \qquad (17)$$

Such an added layer also will increase the second moment of the microcantilever's cross-sectional area, I, making the beam stiffer. Equation 18 shows this effect ($+k$).

$$f_i^{+k} = \frac{\alpha_i^2}{2\pi\sqrt{3}}\sqrt{\frac{k}{M_b} + \frac{3E_{ads}I_{ads}}{L^3 M_b}} \qquad (18)$$

Equation 19 shows the effects of the mass ($+m$) and the thickness ($+k$)

$$f_i^{+m,+k} = \frac{\alpha_i^2}{2\pi\sqrt{3}}\sqrt{\frac{k}{M_b + \Delta M} + \frac{3E_{ads}I_{ads}}{L^3(M_b + \Delta M)}} \qquad (19)$$

where the adsorbed layer (denoted by subscript "ads") has elastic modulus E_{ads} and second moment I_{ads} are given by eq 20 via the parallel axis theorem.

$$I_{ads} = \frac{w t_{ads}^{\ 3}}{12} + w t_{ads}\left[\left(\frac{t_{ads}}{2}\right) - t_b - y_{cm}\right]^2 \qquad (20)$$

The centroid of the cross section including the adsorbed layer is given by eq 21

$$y_{cm} = \frac{E_b t_b^{\ 2} + E_{ads}(2t_{ads}t_b + t_{ads}^{\ 2})}{2E_{ads}t_{ads} + 2E_b t_b} \qquad (21)$$

where t_b is the beam thickness and t_{ads} is the thickness of the adsorbed layer.

The effect of surface stress ($+\Delta\sigma$) effect is given by eqs 22 and 23

$$f_i^{+\Delta\sigma} = \frac{(\alpha_i^{\Delta\sigma})^2}{2\pi\sqrt{3}}\sqrt{\frac{k}{M_b}} \qquad (22)$$

$$\alpha_i^{\Delta\sigma} = \alpha_i\left[1 + \frac{2\sigma L^3}{\pi^2 EI^3}\right]^{1/4} \qquad (23)$$

where σ is the surface stress. Equations 22 and 23 can be rearranged to allow calculation of surface stress based on the resonant frequency for a microcantilever of rectangular cross section (L, w, and t) as shown in eq 24.[7,31]

$$\sigma = \left[\left(\frac{f_i^{+\Delta\sigma}}{f_i}\right)^2 - 1\right]\frac{\pi^2 E w t^3}{24L^3} \qquad (24)$$

One can combine eqs 19, 22, and 23 to arrive at the most general case of a change in frequency due to adsorbed mass ($+m$), to increased stiffness due to a change in thickness ($+k$), and to surface stress ($+\Delta\sigma$); see eq 25.[18,20,37]

$$f_i^{+m,+k,+\Delta\sigma} = \frac{(\alpha_i^{\Delta}\sigma)^2}{2\pi\sqrt{3}}\sqrt{\frac{k}{M_b + \Delta M} + \frac{3E_{ads}I_{ads}}{L^3(M_b + \Delta M)}} \qquad (25)$$

2.2.5. Effect of Damping Due to Viscous Fluids

For most cases, air is assumed not to affect the operation of the cantilever; hence, the equations derived above are valid for microcantilevers operating in air. If the microcantilever is used in a liquid or gas that does influence its operation, then damping effects will influence the response of the microcantilever.[38] The effect of damping can be estimated by eq 26, which relates f_i^{v}, the ith mode frequency of a beam with density ρ_b oscillating in a vacuum, to f_i^{D}, the frequency when oscillating in, and hence damped by, a fluid of density ρ for a Reynolds number $\gg 1$.[39] This is an inertia-resistance dominated situation, so the resistance is roughly proportional to the acceleration of the cantilever.[40]

$$\frac{f_i^{D}}{f_i^{v}} = \left(1 + \frac{\pi \rho w}{4\rho_b t}\right)^{-1/2} \quad (26)$$

It should be noted that, while the damping effects in air have only a minute effect on the resonance frequency, the effect on the quality factor can be quite dramatic, with Q jumping from the order of 10−100 in air to the order of 1 000−10 000 in vacuum. For flows where the Reynolds number is ≪1 (i.e., damping mainly due to the viscosity of the fluid surrounding the beam), an expression (eq 27) analogous to eq 26 can be derived[23,39]

$$\frac{f_i^{D}}{f_i^{v}} = \sqrt{1 - \frac{1}{4Q_i^2}} \quad (27)$$

where Q_i is the ith frequency quality factor for the damped microcantilever (i.e., submerged in a viscous gas or fluid).

2.2.6. Effect of Air Damping on Quality Factor

The effect of air damping on the quality factor of microcantilevers is discussed in more detail by Newell.[41] He presents a number of expressions for the quality factor for a microcantilever damped by air. The first case is where the pressure is so low that air damping is negligible. Here, the quality factor is independent of pressure and must be determined empirically. The second case is where air damping is the dominant mechanism but the air molecules are so far apart that they do not interact with each other. In this case, the quality factor is given by eq 28

$$Q_i = \left(\frac{\pi}{2}\right)^{3/2} \rho t f_i \left[\frac{\left(\frac{R_0 T}{M_0}\right)^{1/2}}{\frac{1}{P}}\right] \quad (28)$$

where ρ is the density of the microcantilever, t is the thickness of the microcantilever, f_i is the resonant frequency of the microcantilever, R_0 is the universal gas constant, M_0 is the molar mass of the air, T is the temperature, and P is the air pressure.

The final case is where the air molecules do interact with each other, and here one assumes that the air acts as a viscous fluid. Since viscosity will be independent of pressure, the quality factor also is independent of pressure. If one uses Stokes' law for damping, eq 29 results

$$Q_i = \left[\frac{w(E\rho)^{1/2}}{24\,\mu}\right]\left(\frac{t}{L}\right)^2 \quad (29)$$

where w is the width of the microcantilever, t is its thickness, L is its length, and μ is the viscosity of air. Thus, the value of the quality factor is strongly influenced by the media that surrounds the microcantilever.

2.3. Lateral and Torsional Mode Frequency Responses

Until now, only pure bending of a microcantilever beam has been discussed. Lateral (Figure 2b) and torsional (Figure 2c) motions can be modeled in similar manners to those presented above. The results presented here are for undamped microcantilevers. The frequency for a freely vibrating beam deflecting in the jth lateral mode is described by eqs 30 and 31[7]

$$f_j^{l} = \frac{w}{4\pi}\left(\frac{\alpha_j^{l}}{L}\right)^2 \sqrt{\frac{EI}{3\rho_b}} \quad (30)$$

$$\cosh \alpha_j^{l} \cos \alpha_j^{l} + 1 = 0 \quad (31)$$

where the superscript l signifies the lateral mode of deformation. In a similar manner, the sth torsional resonant modes for a freely vibrating beam can be modeled as eq 32[7]

$$f_s^{t} = \frac{2s - 1}{4L}\sqrt{\frac{G\xi}{\rho_b I_p}} \quad (32)$$

where the superscript t denotes the torsional mode of deformation, G is the shear modulus ($G = E/(2(1 + \upsilon))$, I_p is the polar moment of the cross section defined by eq 33[42] for a rectangular cross section beam, and ξ is defined by eq 34. For the approximate solution of eq 34, the reader is referred to the paper by McFarland et al.[7]

$$I_p = \frac{1}{12}(tw^3 + wt^3) \quad (33)$$

$$\xi = \frac{1}{3}t^4\left(\frac{w}{t} - \frac{192}{\pi^5}\sum_{n=1}^{\infty}\frac{1}{n^5}\tanh\frac{n\pi w}{2t}\right) \quad (34)$$

These equations for lateral and torsional modes of deflection can be used to derive situation-specific resonant frequencies in an analogous manner for the bending mode equations shown above, e.g., for added mass, added thickness, and fluid viscosity effects.

2.4. Temperature Effects

Thermomechanical noise (vibration due to thermal agitation) is a consequence of a microcantilever being in thermal equilibrium with its environment. This discussion, taken from Newell[41] and Yasumura et al.,[28] is for an undamped microcantilever; one utilizes the material discussed above to include damping. Energy dissipation in a microcantilever causes the stored mechanical energy to be converted into heat. The interaction of a microcantilever with the many microscopic degrees of freedom in its environment will subject the microcantilever to constant random excitation. The relationship between energy dissipation and random thermal excitation is embodied in the "fluctuation−dissipation theorem" of statistical mechanics. The net result is that, the lower the mechanical Q of the system is, the larger is the noise force. The mean square vibration amplitude associated with a mode of oscillation at temperature T can be determined from the equipartition theorem as shown in eq 35

$$\frac{1}{2}k_B T = \frac{1}{2}k\langle z^2\rangle \quad (35)$$

where k_B is Boltzmann's constant, k is the cantilever stiffness, and z is the microcantilever's deflection. If one assumes that the noise spectrum is white (i.e., frequency independent), then the spectral density $SF = 4kk_BT/\omega_0 Q$ and the force noise (F) in a bandwidth (B) is given by eq 36

$$F_{min} = \sqrt{\frac{4kk_B TB}{\omega_0 Q}} \quad (36)$$

where ω_0 is the cantilever resonance frequency and is equal to $2\pi f_0$. For a simple rectangular cantilever, the minimum detectable force can be expressed by eq 37

$$F_{\min} = \left(\frac{wt^2}{LQ}\right)^{1/2} (k_B TB)^{1/2} (E\rho)^{1/2} \quad (37)$$

where w is the microcantilever's width, t is its thickness, L is its length, E is its Young's modulus, and ρ is its density.

Similarly, the mean square root deflection is given by eq 38.

$$z_{\mathrm{rms}} = \left(\frac{kT}{k_B}\right)^{1/2} = \left(\frac{2kT}{wE}\right)^{1/2} \left(\frac{L^3}{t^3}\right)^{1/2} \quad (38)$$

Equations 37 and 38 can be used to design the sensitivity of microcantilevers, but one can see that very high quality factors are necessary for ultrasensitive devices.

2.4.1. Effect on Material Properties

Many of the material properties of microcantilevers depend on temperature. For example, as the temperature increases, the elastic modulus decreases. The temperature dependence of the elastic modulus of silicon in the high-temperature limit has been modeled semiempirically by eq 39[43]

$$E(T) = E_0 - BT \exp\left(-\frac{T_0}{T}\right) \quad (39)$$

where E_0 is the Young's modulus at 0 K. The constants $B > 0$ and $T_o > 0$ are temperature independent. For aluminum oxide, E_0 is reported as approximately 4.6×10^{12} dyn/cm^2, B as 4.41×10^8 dyn/cm^2, and T_0 as 373 K.[43] The frequency shift of silicon microcantilevers and variations in the Q-factor over a range of temperatures has been studied.[44]

2.4.2. Effect on Geometry

Temperature also affects the geometry of a microcantilever, with an increase in temperature generally being related to an increase in dimensions through a parameter termed the coefficient of thermal expansion (CTE). For example, the thermal expansion of silicon is on the order of 3.2 parts per million (ppm) per °C and those of a polymer are on the order of 50−100 ppm/°C.

As one can see from the discussion in this section, it is critical that calibration and operation of the microcantilever be performed at the same temperature and that the temperature is controlled within very tight tolerances. In the absence of temperature control, differential measurements utilizing pairs of coated and uncoated microcantilevers must be performed.

3. Detection Schemes

Vertical, lateral, or torsional movement of a cantilever changes its position. This movement ranges from several angstroms to a micrometer or more, depending upon the dimensionality of the cantilever and the magnitude of surface stress. In this section, methods for measurement of cantilever deflection are examined.

3.1. Optical Lever

The optical lever method, illustrated schematically in Figure 8, is the most widely utilized method of quantifying static and dynamic cantilever deflections. The method involves reflection of a beam of light off the cantilever onto a segmented photodiode or a position-sensitive detector (PSD). Light emitting diodes (LED) and laser diodes are the sources typically used to generate the beam of light.

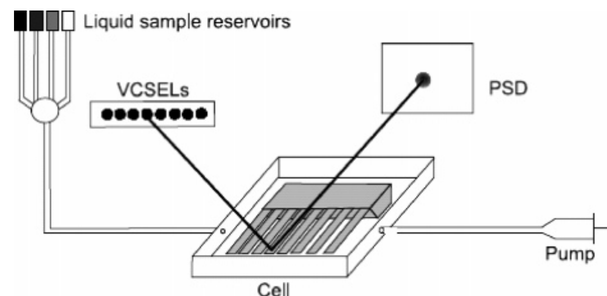

Figure 8. Schematic of the experimental setup with liquid cell, optical readout of cantilever deflections, and sample liquid exchange system: VCSEL = vertical cavity surface emitting lasers, PSD = position sensitive detector. Reproduced with permission from Arntz, Y. et al. *Nanotechnology* **2003**, *14*, 86. Copyright 2003 Institute of Physics Publishing.

Photodiodes, divided into two or four segments, transduce the light energy striking each segment into an electrical signal that can be compared, amplified, and displayed. Motion of the cantilever changes the position of the reflected light beam on the photodiode and, consequently, the level of light energy incident on each segment. Quad-type photodiodes can, in principle, measure all modes of deflection (bending, lateral motion, and twisting) simultaneously. Typically, the reflected beam is centered on photodiode so that each segment has the same level of illumination at the beginning of each experiment. Then, as the cantilever bends, the laser spot changes location on the photodiode array. By comparing the outputs of the segments, the location of the centroid of the reflected laser spot, and, hence, the deflection of the microcantilever, can be determined. Segmented photodiodes are employed extensively in atomic force microscopes.

PSDs are monolithic PIN (positive intrinsic negative) photodiodes with uniform resistance in one or two dimensions. Incident light on the photosensitive region of the PSD generates two photocurrents, each inversely proportional to the distance of the spot from the end of the region. The difference in photocurrents is converted to a voltage, amplified, converted, and displayed. PSDs possess high position resolution and fast response speed and require simple operating circuits. Establishing the relationship between output signal of either segmented photodiodes or PSDs with the magnitude of deflection requires careful calibration.

Optical lever detection is currently the most sensitive method for measuring deflection; vertical deflections as small as a few angstroms can be reliably measured with this technique. An intrinsic limitation of this technique is that the laser diode, positioning system, and detector must be external to the air or fluid stream passing by the cantilever. Their dimensions are large in comparison to the microcantilever. Also, this technique is ineffective when the sample passing over the cantilever absorbs or scatters light, e.g., smoky air streams,[45] and fluids with suspended particles.[46]

The optical lever technique is well-suited for detection of cantilever arrays. A number of formats have been published; two have been commercialized. One approach is to have multiple beam sources and detectors, one pair for each cantilever in the array. While this approach enables simultaneous measurement of all cantilevers in the array, the

integrated source, detector, and signal-processing system is quite complex to design and expensive to manufacture. Sequential reflection of a light beam off each cantilever in the array onto a single detector significantly reduces the complexity of the system and dramatically lowers its cost. One way to achieve this is to scan a single laser source across all of the beams in a cantilever array.[47,48] Another way is to sequentially illuminate each element in an array of LEDs or vertical cavity surface emitting lasers.[11,49−56] A third approach is to illuminate all cantilevers in the array with a single collimated beam, reflecting the light onto the image plane of a charge-coupled device camera.[57,58] Deflection of each cantilever in the array is computed from changes in reflection spot location in images acquired over time.

3.2. Interferometer

Interferometric detection of cantilever deflection is based on constructive and destructive interferences that occur when a collimated beam of light reflects off two surfaces displaced from one another.[59] In the majority of applications of this technique, cantilevers containing a deformable diffraction grating consisting of a reference and movable set of interdigitated fingers were used. These can be intrinsic to a given cantilever or between cantilever pairs. Chemisorption onto the movable set displaces them relative to the reference fingers and alters the intensity of the diffracted orders is altered. The order intensity is measured with a photodiode array. This technique is capable of measuring very small deflections (as small as 0.01 Å)[60] but has a very limited dynamic range. As with the optical lever technique, the interferometric detection technique is ineffective when the sample stream absorbs or scatters the incident or reflected beams. Interferometric detection is being used for high-temperature vibration sensors,[61] while Gimzewski and co-workers[62] used strobed interferometric microscopy to study the different resonance modes of cantilevers in arrays.

3.3. Piezoresistive

The electrical conductivity of a piezoresistive material changes when stress is applied to it. Thus, when a piezoresistive element is integrated onto the cantilever during fabrication, cantilever bending is proportional to the change in resistance. The change in resistance is measured with a Wheatstone bridge, often located at the base of the cantilever.[63,64]

Piezoresistive elements fabricated onto or into cantilevers comprise either semiconductor or metallic strain gauges. A semiconductor strain gauge is smaller and lower in cost than a metallic foil resistance sensor described below. While the higher unit resistance and sensitivity of semiconductor sensors are definite advantages, their greater sensitivity to temperature variations and tendency to drift are disadvantages in comparison to metallic foil sensors. Another disadvantage of semiconductor strain gauges is that the resistance-to-strain relationship is nonlinear, varying 10−20% from a straight-line equation, although this limitation can be overcome through software compensation.

Metallic foil strain gauges measure the change in resistance of a metal as it is stretched. By appropriate calibration, the relation between the strain and the change in resistance can be determined and used to determine the strain in the substrate. The gauge factor (GF) of a material is used to characterize its strain sensitivity and is defined by eq 40

$$\mathrm{GF} = \frac{\Delta R/R}{\Delta L/L} \tag{40}$$

where ΔR is the change in resistance, R is the initial resistance, ΔL is the change in length, and L is the initial length. The numerator is also known as the strain. The relation between strain and resistance change is linear. The application of thin, narrow gold traces to a microcantilever similarly can be used to measure its deflection.

Piezoresitive detection is the second most common technique used for measuring cantilever deflection, even though its sensitivity is less than that of the optical lever.[55] It is applicable to cantilever arrays of almost any size. The read-out electronics can be integrated onto the chip containing the cantilever array. This technique is unaffected by light-absorbing or scattering components in the analyte stream. Because current is flowing through the cantilevers while measurements are being made, local heating can occur. It can be manipulated by changing the amount of current flowing through the resistive layer.[60] Other drawbacks to this technique are thermal, electronic, and conductance fluctuation noise, thermal drifts, nonlinearity in piezoresponse, and poor sensitivity.[45]

3.4. Capacitive

In this detection mode, the cantilever acts as one of the parallel plates of a capacitor. As the cantilever deflects, the distance between the two plates changes and this changes the capacitance of the system. The advantage of capacitive detection is in the simplicity of the associated electronics.[65] This technique is not one of the more common ones used because of a number of limitations. To accurately record cantilever deflection, the dielectric material between the conductive plates must be constant throughout the experiment. The presence of analyte within the gap often changes its effective dielectric constant. Additionally, if the parallel plates are brought in too close proximity, they may stick together, which terminates the collection of useful data until they become separated. This phenomenon is frequently encountered when solvent vapor is passed over the cantilever and the solvent condenses onto the surfaces. Also, although the capacitive cantilevers can be integrated onto a microchip,[66] scaling down the size of the capacitive cantilever will lower its overall sensitivity because the capacitance of a capacitor is directly proportional to its surface area. For gas sensing, Amirola and co-workers[67,68] used capacitive detection of gaseous molecules and found the limit of detection (for their specific cantilever set up) to be 50 ppm for toluene and 10 ppm for octane. Verd and co-workers report sensitivity on the order of 10^{-8} g for their specific capacitive cantilever system.[69]

4. Design, Materials, and Fabrication

Fabrication of cantilevers is an attractive option for groups with the appropriate resources, facilities, and time available. Creating cantilevers in-house allows greater flexibility in the design of the cantilever to enhance its suitability for the intended application. Only recently have commercial sources for cantilever arrays become available (see, for example, the following websites: http://www.concentris.ch; http://www.micromotive.de/Octosensis_e.php; and http://www.cantion.com). This section examines the interplay between the shape of the cantilever, the material from which it is made, and

the fabrication methods required to achieve cantilevers with desired mechanical properties.

4.1. Design Considerations

The shape of the cantilever often depends upon the detection technique. For example, square pads on the end of cantilever beams are used with capacitive detection systems to increase sensitivity because the measured capacitance is proportional to the surface area of the parallel plates.[70] Piezoresistive cantilevers are often U-shaped, with components of the Wheatstone bridge circuit manufactured at their base points.

For optical detection schemes, rectangular, paddle, and T-shaped cantilevers are quite common. However, as pointed out by Mertens and co-workers[48,71] and previously in the Theory of Operation section, the actual cantilever deflection does not agree exactly with Stoney's equation, especially when the shape of the beam is different from that which Stoney used in deriving his equation. The implicit assumption behind the equation is that surface stress will cause a uniform curvature of the beam. Because the cantilever beam is clamped on one end, the surface-stress induced curvature is not uniform, and this can cause the beam to twist.[48] To reduce cantilever torsion caused by the additional stress at the clamped end, Plaza et al. used T-shaped microcantilever arrays.[72] The "T" allows the major part of the beam to be mechanically decoupled from the twist-inducing stress at the clamped end.

4.2. Fabrication of Silicon-based Cantilevers

The microfabrication process for silicon-based (i.e., silicon, silicon nitride, and silicon dioxide) cantilevers comprises four main techniques that, when used in combination, yield multiple cantilever chips with the desired shape and mechanical properties. These techniques are film deposition, photolithography, etching, and doping,[73] the same as those commonly used in fabricating integrated circuits. The intent of this section is to provide an overview of each technique. For in-depth information, the reader is referred to the review by Hierlemann et al.[73] and Madou's text.[74]

The fabrication process typically begins with a polished monocrystalline wafer of silicon or silicon-on-insulator (SOI).[75,76] SOI wafers are composed of a thick bottom later of single-crystal silicon, a middle silicon oxide layer, and a top layer of single-crystal silicon or silicon nitride.[77] SOI wafers are useful because the buried oxide layer acts as an etch stop during the fabrication process. The thin top layer of single-crystal silicon (or silicon nitride) is commonly used as the material of the actual cantilever, so it is important that the defects in this layer are minimized.[75-77]

4.2.1. Film Deposition

Deposition of thin films onto the wafer is carried out by spin-coating, either chemical (CVD) or physical (PVD) vapor deposition, and electroplating. Spin-coating is useful for the formation of polymer thin films, most commonly photoresist, whose utility is described in the next section. The wafer to be coated with the polymer is placed onto a vacuum chuck, which holds it in place. An aliquot of photoresist is dropped onto the wafer, and then the wafer is rotated at thousands of rotations per minute to distribute the polymer evenly over the wafer. Generally, spin-coated polymer thin films have thicknesses of 1−2 μm.[74]

CVD is used to deposit silicon oxide and silicon nitride layers that can be used as insulation, masks, and etch-stops.[73,74] In CVD, gaseous reactants are introduced into the vacuum chamber containing a heated wafer substrate. A thin layer is deposited onto the heated substrate via thermally induced reaction. Depending on the material deposited, CVD films can range in thickness from 20−1500 nm.[73]

Metals are generally deposited using PVD, i.e., sputtering and evaporation.[73,74] In a PVD process, a thin film accumulates on the substrate from a heated reservoir of material in a linear alignment. Metal also can be deposited through electroplating. Metals are useful as reflective surfaces, electrode material, electronic interconnects, thermistors, and chemically reactive binding sites (because alkanethiols covalently bind to gold).

4.2.2. Photolithography

Photolithography is the process used to transfer a pattern onto the wafer. First, a thin film of a UV-active polymer in a volatile solvent (i.e., photoresist) is placed on the wafer by spin-coating. Excess solvent is evaporated by heating the wafer in an oven. Next, a glass plate with transparent and opaque regions (mask) that contains the desired pattern is placed close to the wafer; then the mask and wafer are exposed to UV light. Depending upon the tone of photoresist used, UV light exposure initiates chemical bonding between adjacent polymer strands (cross-linking) or chemical bond cleavage along a strand. The reaction is completed as the wafer is placed in the oven for the postbake. Placement of the exposed photoresist wafer into a developer solution dissolves away the uncross-linked polymer and products of the chemical bond cleavage reaction. Etching is the final step that transfers the pattern from the photoresist onto the wafer. The remaining photoresist protects the underlying wafer from the etchant. After the wafer has been etched, the remaining photoresist is removed.

4.2.3. Etching

Etching is a process used to remove parts of a thin film or the wafer. There are many different etching reagents; both liquid and dry etchants are available. The specific chemicals used for etching are chosen so that they preferentially etch one type of material over another. This way, thin film layers of various materials can prevent certain features of the wafer from being etched and transfer the desired pattern onto the wafer.

4.2.4. Doping

Doping refers to the process of introducing specific impurities into the silicon lattice to alter the electrical conductivity of the silicon. Ion implantation and thermal diffusion are two methods of doping. The type of doping describes whether the dopant contains more or less valence electrons than silicon. For example, incorporation of boron or gallium into the silicon lattice results in p-type doping. These elements have one less electron than silicon; at their location in the lattice, a "hole" is momentarily created. Similarly, incorporation of phosphorus or arsenic into the lattice results in N-type doping. These elements have one more valence electron than silicon; at their location in the lattice, an unpaired electron resides. The unpaired electron and hole are charge carriers and can move about the lattice. Thus, the resistivity of the silicon wafer is determined by

the dopant type and concentration. Doping is commonly employed in piezoresistive cantilevers.

The actual fabrication sequence depends upon the intended use and detection scheme. Silicon-based cantilevers used in optical detection schemes require fewer fabrication steps than those used in piezoresistive, piezoelectric, or capacitive detection schemes. For optical detection schemes, sequences of film deposition, photolithography, and etching are used. A reflective coating often is evaporated onto the surface of the finished cantilever beam to enhance the reflectivity of the beam. Silicon cantilevers used in piezoresistive, piezoelectric, and capacitive detection schemes require more fabrication steps because the detection mechanism is integrated onto the cantilever or the chip holding the cantilevers. Piezoresistive cantilevers require doping in specific areas to create the resistors of a Wheatstone bridge. Detailed information concerning the fabrication sequence and process optimization is readily available in the literature for piezoresistive cantilevers,[78−82] piezoelectric cantilevers,[83−90] and capacitive cantilevers.[68−70,91,92] The number of steps can be reduced by use of silicon-on-insulator (SOI) wafers as the starting substrate.[76,77,93] SOI wafers are composed of a thick bottom later of single-crystal silicon, a middle silicon oxide layer, and a top layer of single-crystal silicon. These wafers are commercially available in a variety of layer thicknesses and dopant levels. SOI wafers are useful because the buried oxide layer acts as an etch-stop during the fabrication process. The thin top layer of single-crystal silicon is commonly used as the material of the actual cantilever, so it is important that the defects in this layer are kept at a minimum.

4.3. Fabrication of Polymeric Cantilevers

Microcantilevers fabricated from polymers inherently possess readily tailorable mechanical and chemical properties. To alter the stiffness of silicon-based cantilevers, their geometry must be changed or a rigid coating must be applied to the surface. In contrast, the stiffness of polymeric cantilevers requires only a change in material. In this way, microcantilevers with the same geometry but different properties can be produced. This reduces manufacturing costs and simplifies the apparatus required for detection. The materials used for polymer-based cantilevers span a wide range of thermosets, thermoplastics, and polymeric composites. Examples of polymer composites include silver nanoparticles and SU-8,[94] carbon nanotubes, poly(*m*-phenylenevinylene-co-2,5-dioctoxy-*p*-phenylenevinylene),[95] and many other combinations.

Polymeric microcantilevers can be fabricated in a variety of ways; the method used is determined by the type of polymer to be used. For example, microcantilevers have been fabricated out of SU-8, a photopolymerizable epoxy−acrylate polymer. The process for fabricating SU-8 cantilevers is quite similar to that used for silicon-based cantilevers. A thin film of SU-8 is deposited onto a wafer by spin-coating. Photolithography then is used to define the regions that will comprise both the cantilever and the chip to which it is attached. The unwanted material is removed and the polymer cantilevers are released from the substrate by immersion in appropriate solvent. SU-8 cantilevers have been made into arrays for optical lever[96−98] and piezoresistive[99,100] detection schemes.

Calleja et al. compared the deflection of silicon nitride cantilevers to SU-8 cantilevers with similar dimensions.[96] When a surface stress change of 1 mN/m was applied to the

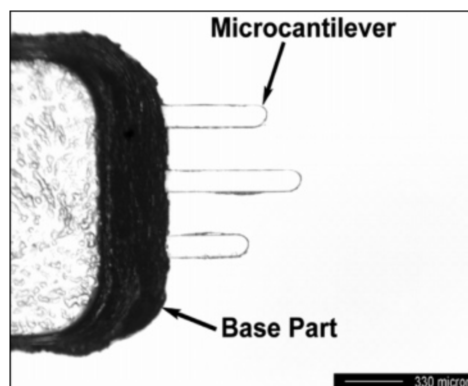

Figure 9. Photograph of polymer microcantilevers produced by injection molding.

SU-8 cantilever, a deflection of 11 nm was observed using optical lever detection. When the same stress was applied to the silicon nitride cantilever, a deflection of only 1.2 nm was measured. On the basis of a minimum detectable deflection of 0.5 nm, Calleja et al. concluded that SU-8 cantilevers could be used to detect surface stress changes as small as 60 μN/m.

Injection molding, an economical, mass production technique, has also been used to fabricate microcantilevers out of thermoplastic polymers.[15,18,37,101] In this process, a molten polymer is forced under pressure into a steel cavity (mold); the shape of the cavity defines the dimensions of both the base and the cantilever(s), as shown in Figure 9. Microcantilevers with thicknesses down to 2 μm and lengths of up to 500 μm have been produced. Because of the small size of microcantilevers, the mold must be heated to the temperature of the molten polymer to ensure mold filling. Any thermoplastic polymer material can be formed into microcantilevers with injection molding; examples include polystyrene, polypropylene, liquid crystal polymer, polymethylmethacrylate, and nanoclay-filled nylon. Cantilevers with tips also have been molded in this manner.[101] Injection-molded microcantilevers have been shown to be of equal caliber to commercial silicon microcantilevers. McFarland and coworkers[15,18,37,101] detail the fabrication of injection-molded microcantilevers. Despite their advantages over silicon-based cantilever arrays, polymeric cantilever arrays are not commercially available.

5. Chemical Selectivity

To achieve selectivity in response, one or more surfaces of the cantilever must be modified to promote binding of desired analytes to the surface and inhibit interfering substances from doing so. A variety of approaches have been used to impart selectivity to microcantilever sensors. The efficacy of a specific approach depends, to a large extent, on the complexity of the sample matrix in which the sensor is used and the chemical reversibility of analyte binding to the cantilever coating.

For detection of a gaseous analyte in an air stream, metallic or ceramic films with a high affinity for the analyte are useful. When all surfaces of the cantilever are coated with a selective thin metallic or ceramic film, then the concentration of analyte in the air stream is proportional to the change in frequency. When only one side of the cantilever is laden with the selective thin film, then the concentration of the analyte in the air stream is proportional to the extent of deflection. Thin metallic or ceramic films are applied to the

desired surfaces of the cantilever using the film-deposition technique described above. To prevent delamination, an intermediate adhesion-promoting layer is often employed. As an example, if a thin film of gold is to be applied to one side of a cantilever by evaporation, then a thin underlayer of titanium or chromium is used to promote adhesion of the gold film onto the silicon cantilever. Mercury vapor in air chemisorbs onto gold films with high affinity.[5,102−104] Known interfering substances include water vapor and volatile organic compounds, which bind to either the gold or mercury surface (e.g., thiols and nitriles). Thus, high fidelity detection of mercury vapor in air is possible with a *single* gold-coated cantilever sensor only when the air stream has been dried and scrubbed of these interfering substances.

The chemical selectivity of metallic and ceramic surfaces is significantly diminished in fluid. To enhance selectivity, several research groups have self-assembled monolayer films onto one or more faces of the cantilever. Reactive terminally substituted thiols, silanes, and siloxanes are commonly used to impart specific chemical functionality to the surface. The choice of reactive group depends upon the cantilever surface composition; the choice of terminal group depends upon the specific chemical interaction desired to attract the analyte to the cantilever surface. While this approach is effective in creating densely packed films on the surface, the analyte binding capacity is limited.

Construction of multilayer films, through self-assembly, dip-coating, or spin-coating, is one means of increasing the capacity of the chemically selective film. Examples of this approach in the literature include the use of trialkoxysilanes,[105−107] cyclodextrins,[108−110] hydrogels,[111−118] and polymers[119,120] as chemically selective coatings. While the capacity of the film increases with increasing film thickness, as the film thickness increases, the following occur:

• The rate of analyte transport into and out of the film diminishes, thereby slowing the temporal response of the sensor.

• The added mass changes the effective spring constant of the cantilever—the degree of change depends upon the uniformity of coverage of the film on the cantilever.

• The viscoelastic response of the film impacts the temporal response of the cantilever and its *Q* factor.

• The number of compounds that partition into the coating increases, thereby reducing the chemical selectivity of the film.

Thus, there is a clear tradeoff between film capacity and both detection specificity and temporal response. The impact of this tradeoff is minimized through the use of arrays in which each cantilever in the array has a different coating. A variety of coatings are available; the identification of the most appropriate coatings for detection of specific analytes in either gas or fluid streams has been aided by the application of chemometrics to this field.[42,49,121−125]

Perhaps the most promising area for development and application of cantilever sensing technology is biology. Deliberate attachment of biological molecules to a cantilever surface opens the possibility of highly selective interactions between the capture molecule and its binding partner. The large number of highly selective binding pairs in biology suggests that, through judicious selection of the coating, cantilever sensor systems can be designed to detect single analytes in complex media with high fidelity. The challenges in creating chemically selective biofilms lie in the following: controlling the spatial distribution and orientation of capturing agent; minimizing the nonspecific binding by components in the sample matrix to the cantilever; maximizing the chemical sensitivity and dynamic range in sensor response; and extending the time before the capture agent denatures, thereby eliminating selectivity in cantilever response.

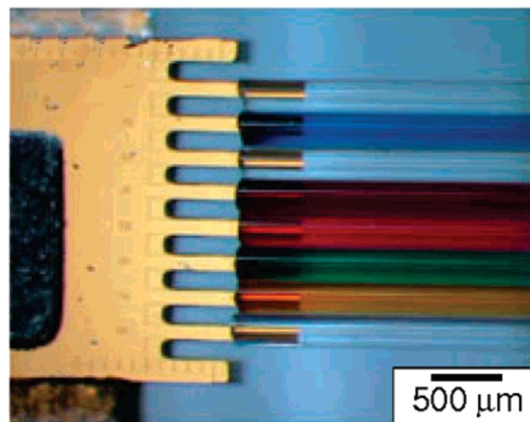

Figure 10. Immersion of a cantilever array into an array of glass microcapillaries filled with food coloring for demonstration purposes. Reproduced with permission from Bietsch et al. *Nanotechnology* **2004**, *15*, 873. Copyright 2004 Institute of Physics Publishing.

Various approaches for immobilizing capturing agents on cantilever surfaces have been published. Most involve covalent attachment of the biomolecule directly to the cantilever surface or through a hetero-bifunctional linker molecule (e.g., alkanethiol or -siloxane). The use of a linker facilitates uniform distribution of biomolecule on the surface and minimizes denaturing caused by interactions with the cantilever surface. Blocking agents (e.g., polyethylene glycol and bovine serum albumin) typically are employed to reduce nonspecific binding. Further details regarding biomolecular coatings on cantilevers are provided below in the Biologicial Applications section.

Coating individual cantilevers within arrays can be challenging. One way is to insert the desired cantilever into a capillary filled with reagent using a micromanipulator.[51] The capillary must have an internal diameter larger than the width of the beam, and the wall of the capillary must be thin enough to fit between the cantilever beams in the array. The capillary is held in place for an allotted amount of time required for functionalization and then retracted. When several different cantilevers within the array require functionalization, this approach becomes time-consuming and tedious.

Three approaches have proven useful for functionalizing multiple cantilevers: capillary arrays, inkjet printing, and contact printing. All cantilevers within the array can be simultaneously inserted into an array of capillaries (or small-volume reaction wells) using an appropriately designed micromanipulator (see Figure 10).[126,127] All sides of the cantilever are wetted using this approach. Thus, if only one side of the cantilever is to be modified, then the reaction chemistry of the fluid within the capillary must be designed to react only with the desired region (e.g., photochemically initiated reaction). Inkjet printing is also useful for coating individual cantilevers within an array.[128,129] Commercial micro-inkjet printing systems are available from several manufacturers (e.g., Cantisens and Microdrop Technologies). Micro-inkjet printing affords efficient and controlled functionalization of only one side of the cantilever (see Figure

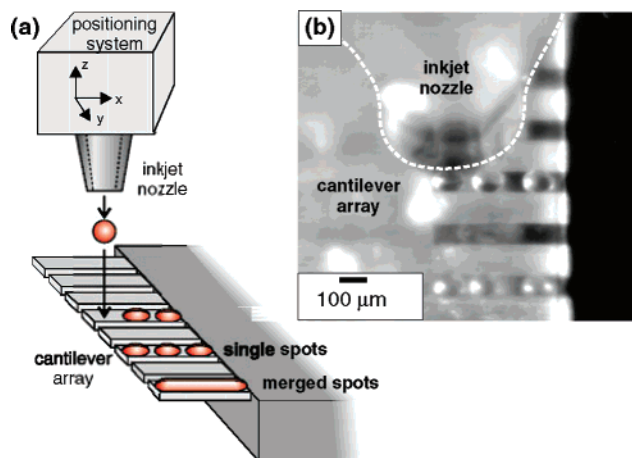

Figure 11. Inkjet printing of individual droplets onto a cantilever array: (a) schematic and (b) image from a video camera. A positioning system allows accurate placement of single droplets onto selected cantilevers. Reproduced with permission from Bietsch et al. *Nanotechnology* **2004**, *15*, 873. Copyright 2004 Institute of Physics Publishing.

11), and it is faster than the capillary array. Coatings also can be applied by contact-printing methods using dip-pen lithography[130−134] or specially designed stamps.[135,136] Commercial dip-pen lithography systems are available (e.g., BioForce, NanoInk, and Nanonics Imaging).

6. Chemical Applications

Numerous applications of chemomechanical sensors in environmental monitoring, medical diagnostics, and chemical detection in air and flowing liquids have been published. Several reviews have been published over the past decade.[55,60,137−144] This section highlights recent and innovative applications. Because of editorial restrictions on the number of citations, the work cited herein illustrates only some of the applications currently being explored. Our selections are, without doubt, subjective.

6.1. Volatile Organics

In a series of papers emanating from IBM Zurich, the University of Basel, and the Paul-Scherrer-Institute, the efficacy of cantilever arrays for detection of specific analytes in complex gaseous mixtures has been demonstrated. Lang and co-workers[11,50,145] showed that the diffusion of various alcohols into polymethylmethacrylate coating induces resonance frequency shifts and differential bending of cantilevers.

Baller et al.[49] coated each cantilever in the eight-cantilever array with a specific polymer layer to transduce a physical process or a chemical reaction into a nanomechanical response. Chemisorption of the analyte induced polymer swelling; the kinetics of the swelling process was related to the vapor pressure and the solubility characteristics of the analyte in the polymers. The array format enabled the use of some cantilevers as reference sensors. Baller et al. distinguished different mixtures of alcohols using principal component analysis (PCA) with mixtures that had been previously characterized. They could not determine the mixing ratio of individual analytes directly from the cluster positions of the mixture's constituents in the PCA plot because desorption kinetics of analyte mixtures do not depend on the mixing ratio in a predictable way. A year later, the same group demonstrated the simultaneous detection of deflection and resonant frequency shifting of cantilevers within the array to the same analytes.[42] Using artificial neural network analysis of the deflection and resonant frequency shift data, they demonstrated the utility of polymer-coated cantilevers for both qualitative and quantitative analysis of gaseous mixtures with well-defined composition.

In related work, Betts and co-workers[119] evaluated two polymeric chromatographic stationary phases as cantilever coatings for select vapor phase analytes. Fagan et al.[107] evaluated sol−gels as cantilever coatings for nonpolar vapor phase analytes. Maute and colleagues[146−149] used polydimethylsiloxane, polyetherurethane, zinc phthalocyanine, and ethyl cellulose as coatings for the detection of volatile organic compounds in the gas phase. Differential chemisorption of analytes into each polymer film and principal component analysis of the response of each cantilever to the analyte provided a means of qualitative and quantitative determination. Improved performance was found when using higher resonant modes for detection.

Headrick et al.[109] used focused ion milling of the cantilever surface to create submicron channels across the width of one side of the cantilever. Responses of the nanostructured, coated cantilevers to a series of volatile organic compounds were compared to smooth, coated cantilevers. The results showed that roughened cantilevers were more sensitive, i.e., exhibited an increase in differential stress to the analytes investigated.

Lange et al.[150] compared the performance of cantilever arrays to thickness shear mode resonators and to surface acoustic wave devices to detect volatile organic compounds in vapor phase. From parallel analyses performed by these transducers on a mixture of *n*-octane and toluene, it was shown that the limit of detection achieved with cantilever sensors is comparable to that of other acoustic wave-based gas sensors.

To enable improved quantification of analyte mixtures, Kurzawski et al.[151] evaluated the performance of a single-chip, three-transducer, complementary metal oxide semiconductor gas sensor microsystem. This system comprised a mass-sensitive cantilever, a thermoelectric calorimetric sensor, and an interdigitated capacitive sensor. Each sensing element was coated with various partially selective polymers and then was exposed to different volatile organic compounds. The sensitivities of the three different polymer-coated transducers to defined sets of gaseous analytes were determined. These workers have demonstrated that each transducer responds to fundamentally different molecular properties. Thus, the response of each transducer to an analyte provides orthogonal data from which analytes present in the mixture can be quantified, using appropriate signal-processing and pattern-recognition techniques.

Fadel et al.[26,152] investigated the analysis of gaseous mixtures using piezoresistive cantilevers of millimeter dimensions. They showed that the choice of the cantilever dimensions and the polymer thickness for gas detection requires compromises concerning sensitivity, response time, quality factor, and resonant frequency. Their comparison between millimeter-size and micrometer-size cantilevers shows the importance of noise in the design of an integrated sensor.

The Ziegler group[8,153] showed that electrostatic or magnetic actuation of the cantilever results in the enhancement of the quality factor by over 3 orders of magnitude for commercial cantilevers. With actuation, cantilever sensors possess a 1000-

fold higher mass sensitivity compared to quartz crystal microbalances.

6.2. Chemical Warfare Agents

Cantilever technology has been applied to detect chemical warfare agents.[154−159] Most published reports have centered on detection of the nerve agent simulant dimethylmethylphosphonate in their studies. Limits of detection were in the 0.5−20 ppb range, depending upon the coating used and the detection mode.[160−164] In only a few instances has the selectivity of detection been investigated.[165] Assessment of the practical utility of this sensing technology for chemical warfare agent detection awaits a systematic study of the selectivity of coatings to common components found in the atmospheres of cities and on the battlefield.

6.3. Explosives

Two approaches have been explored in developing cantilever sensors for detection of explosives: deflagration of particles placed on the cantilever[155,166−168] and chemisorption of vapor into thin coatings on cantilevers. The low volatility of most explosives limits the utility of the latter approach and sensitivities obtained to date are less than those of competitive technologies.[169−171]

6.4. Toxic Metal Ions

The concentration of a variety of metal ions in solution has been determined using cantilever technology. For metal ions that chemisorb (or amalgamate) with the metallic coatings used to increase reflectivity for optical lever measurements of cantilever detection, quantization of metal ion concentration is straightforward (e.g., detection of Hg^{2+} with gold-coated cantilevers).[172] For other metals, cantilever deflection can be induced through ion exchange of the analyte onto thin film coatings. For example, the concentrations of Cr^{2+}, Ca^{2+}, Cs^{+}, and CrO_4^{2-} can be determined via ion-exchange with ω-modified alkanethiol monolayers self-assembled onto gold-coated cantilevers.[123,173−175] In some instances, very low limits of detection are obtained (e.g., Cs^{+} and CrO_4^{2-}), whereas in others (e.g., Ca^{2+}), the limit of detection, dynamic range, and selectivity of the method are not competitive with ion-selective electrode technology.[173,175] Hydrogel coatings can also be used in quantifying metal ion concentrations.[116,117] Monolayers composed of alkanethiols modified with crown ethers have proven to be an effective way to improve selectivity and sensitivity for specific ion detection.[175]

7. Biological Applications

7.1. Cells

In 2001, Ilic and co-workers[176] first reported the detection of *Escherichia coli* cells using a cantilever array. Selective binding to the cantilever was achieved with the anti-*E. coli* antibodies immobilized onto the cantilever. Resonant frequency shifts correlated with the number of cells bound to the surface. The sensitivity of the method was sufficient to detect the binding of a single cell. These findings were confirmed by Zhang and Ji.[177] Campbell and Mutharasan[178] extended the work of Ilic and co-workers, showing that a composite self-excited cantilever made of a PZT film and glass of a few millimeters in length and coated with anti-*E. coli* antibodies can be used to detect *E. coli* O157:H7 in fluid. Sensitivity achieved was in the order of tens of nanograms, with a limit of detection of only 700 bacterial cells/mL.[179]

Gfeller et al.[180,181] demonstrated that an oscillating cantilever can be used as a sensor for active bacterial growth. Their approach was elegant in its simplicity. *E. coli* cells were deposited onto cantilevers coated with a thin nutritive agarose layer and kept in a humid environment. Within minutes, the cells started to grow and assimilate water, protein, salts, and carbohydrates from the nutritive layer. To regain equilibrium with the humid environment, the nutritive layer absorbed water; the resultant mass increase produced a commensurate shift in resonant frequency. When they compared the observed frequency shifts due to additional mass loading onto the cantilevers with a conventional bacterial growth curve, all characteristic bacterial growing phases were observed. By incorporation or omission of antibiotics in the cantilever coating, they demonstrated the utility of their approach for rapidly assessing antibiotic resistance. This new application of cantilever array technology offers numerous advantages over conventional bacterial detection methods including rapid real-time detection, label-free and small analyte volume, and high sensitivity.

Ramos and co-workers[182] recently showed that the response of oscillating cantilevers to bacteria adsorption depends on the added mass, the site of immobilization of the cell on a cantilever, and the stiffness of the bacterial cells. They predicted that detection sensitivities can be increased by an order of magnitude or more by monitoring higher vibrational modes or scaling down cantilever size. However, the mechanical properties of adsorbed molecules became increasingly important as the size of the resonator was decreased. Taken collectively, these reports portend of the use of microcantilever-based sensors for detection of pathogenic bacteria in medical diagnostics and monitoring of our food supply.

7.2. Viruses

Ilic et al.[183] first reported on the use of cantilever arrays to detect immunospecific binding of viruses, captured from liquid. Baculovirus particles bound selectively to an AcV1 antibody monolayer immobilized onto the cantilever surface. The resonant frequency shift resulting from the adsorbed mass of the virus particles distinguished solutions of virus concentrations varying between 10^5 and 10^7 pfu/mL. Single virus particle detection was achieved using specially designed cantilevers. Similar findings were reported by Gupta and co-workers[184] using vaccinia virus, a member of the *Poxviridae* family and the virus that forms the basis of the smallpox vaccine.[185] Ji and co-workers[159] showed the utility of antibody−antigen binding interactions for detection of bio-warfare agents ricin and tularemia.

Dhayal and co-workers[130] demonstrated the utility of peptide-functionalized silicon cantilever arrays for detection of whole *B. subtilis* spores (a nonpathogenic *B. anthracis* simulant) in liquids. Real-time detection was achieved by monitoring stress changes in the cantilever due to spore binding. Estimates for the induced stress per binding event were obtained. They also observed a higher sensitivity to resonant frequency shifts by monitoring with the fifth mode of vibration. There results suggest that real-time detection of multiple pathogenic organisms can be realized using peptide-funtionalized microcantilever arrays.

Campbell and Mutharasan[186,187] investigated the detection of pathogen *Bacillus anthracis* spores in liquid under both

stagnant and flow conditions. They reported the detection of *B. anthracis* spores at a very low concentration (300 spores/mL) using piezoelectrically excited millimeter-sized cantilever sensors coated with antibody specific to *B. anthracis*. High selectivity was demonstrated by detecting *B. anthracis* spores in the presence of another Bacillus spore (*Bacillus thuringiensis*) at ratios up to 1/500. More complicated spore mixtures also have been examined.[188] In these, the presence of non-antigenic Bacillus species reduced the binding kinetics of *B. anthracis* spores but did not alter the steady-state response of the sensor.

Nugaeva and co-workers[189] explored the use of cantilever arrays for selective immobilization and rapid detection of fungal spores. Cantilever arrays were exposed to either the mycelial form *Aspergillus niger* or the unicellular yeast form *Saccharomyces cerevisiae*, as models to explore their utility for growth detection of eukaryotic organisms using cantilever arrays. These workers exploited the specific biomolecular interactions of surface-grafted proteins (concanavalin A, fibronectin, or immunoglobulin G) with the molecular structures on the fungal cell surface to achieve selective immobilization of the spores. They found that these proteins have different affinities and efficiencies to bind the spores. Maximum spore immobilization, germination, and mycelium growth were observed on the immunoglobulin G functionalized cantilever surfaces. They also found that spore immobilization and germination of the mycelial fungus *A. niger* and yeast *S. cerevisiae* led to shifts in resonance frequency within a few hours, in contrast to conventional techniques that require several days. Measured frequency shifts were proportional to the mass of single fungal spores, and this biosensor could detect the target fungi in a range of 10^3-10^6 CFU/mL. This work exemplifies an important application of cantilever array technology in medical and agricultural diagnostics and food- and water-quality monitoring.

7.3. Antigen–Antibody Interactions

Raiteri and colleagues[60] reviewed the working principles behind cantilever-based sensors based on antigen−antibody interactions. The reader is referred to this review for a critical analysis of the literature in this area up through the year 2000. Several reports have appeared over the last 7 years that utilize antigen−antibody binding for selectivity. For example, Arntz et al.[51] presented continuous label-free detection of two cardiac biomarker proteins, creatine kinase and myoglobin, using anti-creatine kinase and anti-myoglobin antibodies covalently anchored to a cantilever array. Binding of the antigen to the anchored antibodies generated sufficient surface stress to enable detection via cantilever deflection. Both myoglobin and creatine kinase could be detected independently using cantilevers functionalized with the corresponding antibodies, in unspecific protein background. These workers showed the utility of reference cantilevers to eliminate thermal drift, undesired chemical reactions (i.e., nonspecific binding), and turbulence from injection of liquids into the cell. They achieved a sensitivity detection of myoglobin below 20 mg mL^{-1}.

Grogan et al.[190] investigated the activity, stability, lifetime, and reusability of monoclonal antibodies to myoglobin covalently immobilized onto cantilever surfaces. Sucrose was shown to be an effective stabilizing agent for the immobilized antibody layer; with it, the immobilized antibody was found to have a stable active lifetime for up to 7 weeks.

Alvarez and co-workers[191] reported the use of a synthetic hapten conjugated with bovine serum albumin as a bioselective layer for cantilever-based detection of the pesticide dichlorodiphenyltrichloroethane (DDT). Exposure to a solution of a specific monoclonal antibody to the DDT hapten derivative results in deflection of the cantilever. Specific detection is achieved by performing competitive assays in which the cantilever is exposed to a mixture of the monoclonal antibody and DDT.

Backmann and colleagues[192] showed that single-chain Fv (scFv) antibody fragments can be used as receptors to detect antigens by the static deflection of cantilevers. The authors reported that the performance of the microcantilever-based immunosensor was comparable with surface plasmon resonance. By simultaneously tracking deflection of sensing and reference cantilevers, the differential deflection signal revealed specific antigen binding and was proportional to the concentration of antigen in solution.

Dutta et al.[193] reported the first demonstration of chiral discrimination using microcantilever sensors. Stable, reusable protein bioaffinity phases based on unique enantioselective antibodies were created by covalently linking monoclonal anti-D− and anti-L-α-amino acid antibodies to nanostructured cantilever surfaces. The temporal response of the cantilever (Δdeflection/Δtime) was linearly proportional to the concentration of chiral amino acid and allowed quantization of enantiomeric purity up to an enantiomeric excess of 99.8%.

Hwang and co-workers[194,195] have fabricated a self-actuating and self-sensing piezoelectric cantilever for label-free detection of a prostate-specific antigen. Cantilevers were coated with parylene-c, deposited by chemical vapor deposition, to electrically insulate the oscillator circuitry for use in fluids.[196,197] Specificity in detection of PSA was achieved through its binding to a PSA antibody that was immobilized via host−guest interactions with a proprietary calixcrown self-assembled monolayer. The resonance frequency shift of the cantilever was proportional to antigen concentration. This strategy also was used for detection of C-reactive protein.[198,199] Kang and co-workers[200] reported the assay of myoglobin concentration using PZT cantilevers coated with biotinylated myoglobin antibodies immobilized onto the surface through streptavidin conjugation.

Most of the published works in this area focus on demonstrating that specific antigen−antibody pair interactions lead either to mass increases that can be sensed by shifts in cantilever resonance or to changes in surface stress that produce measurable cantilever deflections. Little attention is directed to performing cantilever-based immunoassays in a clinically relevant setting. A noteworthy exception is the work of Wu and colleagues.[201] These authors report the detection of two forms of prostate-specific antigen (PSA) over a wide range of concentrations from 0.2 ng/mL to 60 mg/mL in a background of human serum albumin (HSA) and human plasminogen (HP) at 1 mg/mL. Prostate-specific antigen is a particularly useful marker for early detection of prostate cancer and in patient monitoring for disease progression. In serum, this biomarker exists in two forms: uncomplexed and complexed with the serum protease inhibitor α1-antichymotrypsin. Early diagnosis of prostate cancer requires an accurate measure of both the total concentration and the ratio of the complexed to uncomplexed forms of the antigen in serum. In addition, the clinically useful range spans from 0.01 to >10 ng/mL. The dose-response curve they obtained

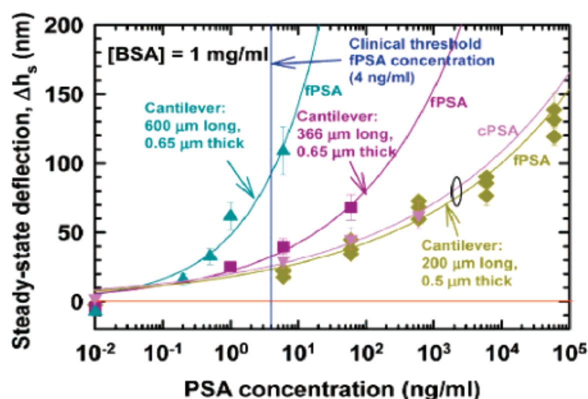

Figure 12. Steady-state cantilever deflections as a function of uncomplexed (fPSA) and complexed (cPSA) prostate specific antigen concentrations for three different cantilever geometries. Reprinted with permission from Wu et al. *Nat. Biotechnol.* **2001**, *19*, 856. Copyright 2001 Nature Publishing Group.

with cantilevers of differing length is shown in Figure 12. This curve was obtained under static conditions that included thermal regulation.

In contrast to the conventional enzyme-linked immunosorbent assay for this antigen, the cantilever-based assay required no labels and was performed in a single reaction without additional reagents. A logical extension of this work involves the use of an array of microcantilevers to perform multiple assays. High fidelity, clinically relevant detection of this biomarker for prostate cancer would be anticipated via the coating of individual cantilevers within the array with antibodies selective for different epitopes on this antigen. A number of such antibodies are now commercially available.

7.4. DNA Hybridization

Fritz and his colleagues[125] pioneered the use of cantilevers for detection of nucleic acid hybridization. Deflection of each cantilever in the array was measured using the optical beam deflection technique. 5′-Thio-modified synthetic DNA oligonucleotides with different base sequences were covalently immobilized on the gold-coated side of the cantilevers the array. When solutions containing the complementary oligo were injected into the liquid cell, hybridization resulted in a change in surface stress between the functionalized gold and the nonfunctionalized Si surface, bending the cantilever. This is shown schematically in Figure 13. This work stimulated interest in exploiting the sensitivity of chemomechanical detection of DNA hybridization. A crucial test for any DNA hybridization sensor is its ability to discern mismatches. Fritz and colleagues[125] observed a small but measurable difference in surface stress between a pair of complementary oligos and a pair with a single base mismatch between two DNA sequences that can be detected.

Hansen and co-workers[202] further evaluated the capability of cantilever sensors for detecting single base mismatches. They found that the direction of cantilever bending, whether tensile or compressive, depended up the number and location of mismatch sites along the strand pairs. Wu et al.[203] showed that the magnitude of cantilever deflection during hybridization depends upon the ionic strength of the matrix. McKendry et al.[127] systematically examined the impact of single strand extensions on cantilever deflection during DNA hybridization. In all cases, compressive surface stress results from hybridization, regardless of whether the complementary

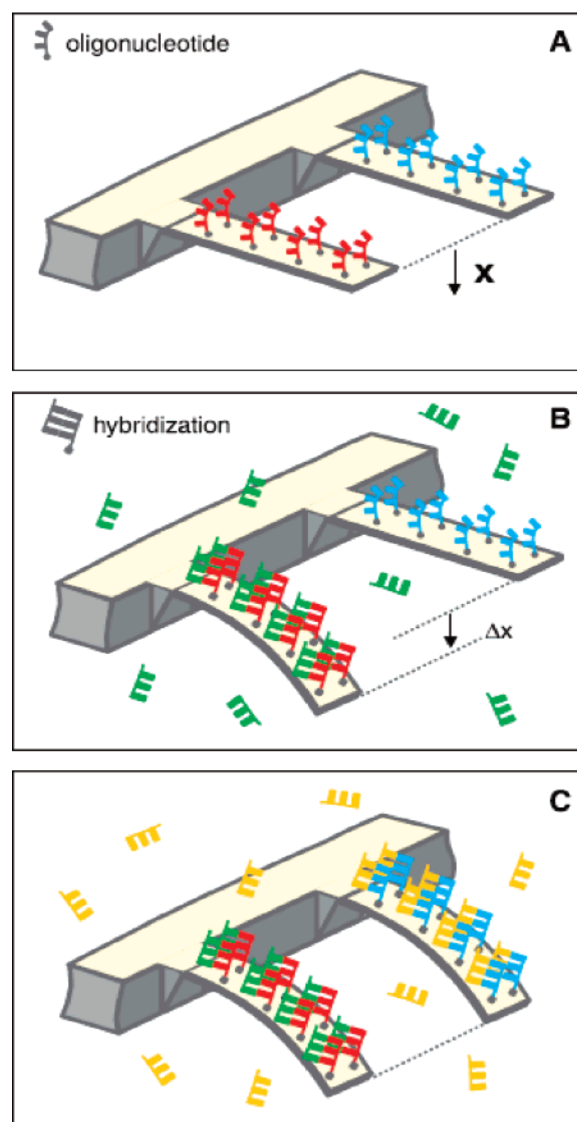

Figure 13. Schematic illustration of the hybridization assay. Each cantilever is functionalized on one side with a different oligo (red or blue). (A) The differential signal is set to zero. (B) After injection of the first complementary DNA strand (green), hybridization occurs on the cantilever laden with the matching sequence (red), increasing the differential signal. (C) Injection of the second complementary DNA oligo (yellow) causes the cantilever functionalized with the second oligo (blue) to bend. Reprinted with permission from Fritz et al. *Science* **2000**, *288*, 316. Copyright 2000 American Association for the Advancement of Science.

oligomers have the same number of nucleotides. They found that hybridization between two complementary 12-mers generated an average compressive surface stress of 2.7 mN/m.

Hagan et al.[204] presented an explanation of cantilever deflections resulting from adsorption and subsequent hybridization of DNA molecules. Using an empirical model, they predicted deflections upon hybridization that are consistent with experimental results. They asserted that hydration forces, not conformational entropy or electrostatics, are the dominant contributors to deflections arising from DNA hybridization. They showed that predicted deflections before and after hybridization strongly depend on surface coverage as well as the degree of disorder on the surface. The latter point was experimentally verified by Alvarez and co-workers.[205]

In a follow-up report from the Majumdar group, Stachowiak et al.[206] provided experimental evidence that the surface stresses resulting from hybridization depend on oligo length, grafting density, and hybridization efficiency. At low ionic strength, the osmotic pressure of counterions dominates the intermolecular forces, while at higher ionic strength, the grafting density is independent of the ionic strength and hydration interactions dominate. They also showed that, regardless of the length and grafting density of the single-stranded probe DNA, surface stress was related exponentially to the density of hybridized DNA. The same group[207,208] observed surface stress changes in response to thermal dehybridization, or melting, of double-stranded DNA oligonucleotides that were grafted on one side of a microcantilever beam. Changes in surface stress occur when one complementary DNA strand melts and diffuses away from the other, resulting in alterations in the degree of hydration and electrostatic interactions between the remaining neighboring surface-grafted DNA molecules. They were able to distinguish changes in the melting temperature of dsDNA as a function of salt concentration and oligomer length.

Recent effort has focused on improving sensor performance. Several groups have evaluated piezoresistive detection of DNA hybridization as an alternative to optical methods.[128,209,210] While piezoresistive detection is less sensitive than the optical lever method, piezoresistive methods are sufficiently sensitive to detect hybridization and single base mismatches. Improvement in sensitivity is anticipated with continued optimization of piezoresistive cantilevers. Others have focused on fabricating cantilevers from polymers in hopes of lowering the limit of detection through reduction in cantilever spring constant without significantly changing the active area.[96,211]

Su et al.[212] used gold nanoparticle modified oligos to improve the mass sensitivity of resonant frequency-based microcantilever detection of nucleic acid hybridization. Their method is capable of detecting DNA concentrations as low as 0.05 nM. As clearly pointed out by Alvarez and co-workers,[205] detection of nucleic acid hybridization requires reference cantilevers sensitized with noncomplementary DNA to decouple the molecular recognition signal from nonspecific binding events and matrix effects.

This highlights the need for an improved understanding of the mechanisms responsible for surface stress due to the biomolecular interactions. Such knowledge is crucial for the development of immobilization procedures in which the geometry of the receptor molecules is addressed to generate high interaction forces between neighboring molecules during molecular recognition.

7.5. Enzymes

Subramanian et al.[213] reported on the first microcantilever-based enzymatic assay. The enzyme glucose oxidase was immobilized onto a gold-coated silicon cantilever with glutaraldehyde following coating of the gold surface with poly-L-lysine. Quantifiable deflection of the cantilever was observed in the presence of analyte. Their analysis of the heat of the enzymatic reaction and the thermal sensitivity of the cantilever suggested that cantilever deflection is not simply a result of reaction-generated heat but appears to result from surface-induced stresses. They offered two hypotheses to account for the surface stress: entropic effects due to the continual binding of glucose at the active site of the enzyme and changes in the local chemical environment that result from glucose conversion to gluconic acid and peroxide.

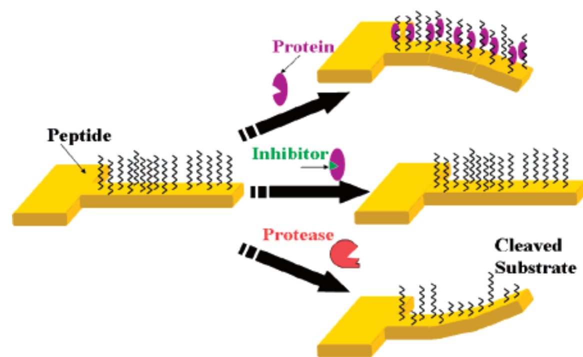

Figure 14. Schematic illustration of protein binding and enzymatic assays with cantilevers.

Yan and co-workers sought to clarify the source of cantilever deflection when immobilized glucose oxidase is exposed to glucose.[214,215] Their immobilization strategy differed from that of Subramanian et al. in that the enzyme was electrostatically immobilized within an alternately charged polyelectrolyte multilayer structure that comprised poly(sodium 4-styrenesulfonate) and polyethyleneimine. The multilayer approach provided improved performance. They proposed that cantilever bending results from both a conformational change of the enzyme in the presence of glucose and from protonation of the polymer multilayer structure as a consequence of the enzyme-catalyzed oxidation of glucose to gluconic acid.

Pei et al.[216] further characterized the performance of a glucose oxidase-based cantilever sensor. They cross-linked the enzyme to bovine serum albumen chemisorbed onto the surface. They concluded that the deflection response of the cantilever cannot be due to the heat of the enzymatic reaction and attributed the deflection mechanism to changes in the local chemical environment of the coating layer. They noted that the poor reproducibility of results for this enzyme-based glucose sensor is likely due to the corrosive nature of peroxide produced by the enzymatic reaction. Clearly, the mechanism behind the surface-induced stress observed for this type of glucose sensor remains unknown.

Bottomley and co-workers reported the use of microcantilevers as sensors of enzymatic function.[217] Exposure of cantilevers coated with enzyme substrates to enzymes capable of changing substrate mass, conformation, and charge results in measurable deflection of the cantilever as shown in Figure 14. Enzyme inhibitors also can be identified using this approach.

Stevenson and colleagues[218] monitored the restriction and ligation of cantilevers coated with DNA. An oligo containing the Hind III restriction site was immobilized on the cantilever and then digested with that enzyme; strand scission produced cantilever bending and left behind a shortened oligo with a single-stranded sticky end. Exposure of a second oligo with a compatible end to the DNA on the cantilever in the presence of ligase resulted in the extension of the immobilized oligo and commensurate cantilever deflection in the opposite direction. The authors point out that, since most DNA restriction and ligation enzymes require dithiothreitol to retain their activity, immobilization of the oligo through thiol linkages must be avoided. Otherwise, displacement of the thiolated DNA from the gold surface by dithiothreitol will produce cantilever deflection and complicate detection of the restriction and ligation events.

Liu and colleagues[219] presented a new approach to track enzyme action with cantilevers. Their technique relies on

the detection of bead detachment from the cantilever due to the enzyme cleavage of the linker tethering the bead to the cantilever. To illustrate this principle, they used the enzymatic action of Botulinum neurotoxin type B on its substratum, the synaptic protein synaptobrevin 2. Nickel−agarose beads were functionalized with recombinant synaptobrevin 2 conjugated to six consecutive His residues at its C terminus. To suspend the bead off the cantilever tip, they used protein−protein interaction (synaptobrevin 2 with another synaptic protein, syntaxin 1A). In the presence of zinc ion, the neurotoxin cleaves synaptobrevin 2, leading to the detachment of the bead from the tip. Since the mass of the bead is many times larger than that of the immobilized protein, its detachment chemically amplifies the mass loss of the protein fragment.

The bead detachment technique is general and can also be used for any cleavage reaction. For example, Weizmann et al.[220] utilized the endonuclease scission of magnetic beads functionalized with sequence-specific DNAs to detect single base mismatch specificity of the endonucleases. Magnetic beads were used to reduce thermal motion and amplify the mechanical motion of the cantilever to enzymatic action. In a subsequent report, they extended this approach to the development of enzyme-based AND or OR logic gates.[221] The bead detachment technique is not limited to cleavage reactions; it is also suitable for displacement reactions, such as in receptor−ligand pairs, where the introduction of one chemical leads to the displacement of another.

8. Recommendations for Future Work

8.1. Guidelines for Reporting Sensor Performance

To facilitate comparison with other sensing platforms, we suggest the following figures of merit be included in all future publications regarding the performance of microcantilever sensors: *detector sensitivity, limit of detection, dynamic range,* and *sensitivity of the analysis*. Within the microcantilever community, the term *sensitivity* is used to describe several different parameters. Some workers use this term to describe the minimum concentration of analyte that can be detected. Others use it to describe the performance characteristics of the sensing technique used to measure shifts in cantilever resonance frequency or changes in cantilever deflection. A third group uses this term to describe the slope of the calibration curve. Multiple usages of the same word can lead to confusion and misinterpretation on the part of the reader.

We suggest more explicit terminology be used in reporting results. The term "*limit of detection*" should be used to describe the minimum concentration of analyte that can be reliably detected. Convention within the analytical chemical community is that this is the concentration that gives a sensor response signal equal to three times the background noise level. The performance of the sensor to changing concentrations of analyte should be reported and distinguished from the sensitivity of the device used to measure cantilever movement. We suggest that the term "*detector sensitivity*", the measured change in signal per unit value of the sensor response, be employed in characterizing device performance. For optical level and piezoresistive detection of cantilever deflection, the detector sensitivities would have units of V/nm and $(\Delta R/R)$/nm, respectively. This term is a function of the properties of the cantilever, the deflection measurement technique, and the signal amplification techniques employed. This figure of merit would be of benefit to those trying to compare cantilever designs, materials, and detection techniques. We suggest that the performance of the sensor to changing concentrations of analyte be labeled "*sensitivity of the analysis*". This parameter is determined from the slope of the linear region of the dose−response curve. As acquisition of this parameter requires exposure of the coated cantilever to varying concentrations of analyte and measurement of the system's response, a measure of the chemical reversibility of analyte binding to the coating is readily obtainable and also should be reported. Similarly, in the course of determining the chemical sensitivity, the experimenters should determine and report the "*dynamic range*" of the sensor for the specific analyte under study. While this issue may seem obvious to the majority of readers, the omission of this information in many of the published papers has made it difficult for us, during the course of writing this review, to evaluate the scientific contribution of many papers and include them in the context of important, new applications of microcantilever sensor technology.

8.2. Experimental Design Considerations

In the first few years following the invention of this sensor technology,[1,3−6,222,223] experimentation with a single cantilever was commonplace. Since then, it has become well-established that cantilevers respond to small changes in temperature, viscosity, and ionic strength of the medium in which they are immersed, as well as to the flow dynamics of the cell that houses the cantilever chip. Thus, the utility of single cantilever experimentation in fluid streams is, at best, questionable. In many instances, interpretation of results of present-day research involving single-cantilever experimentation are based largely on the assumption of fixed conditions between sequential experiments. Often, experiments expressly designed to test the validity of the assumption are unreported.

Microcantilever arrays are the preferred format. They enable control experiments to be performed simultaneously with analyses and provide more reliable control of empirical factors such as thermal drift, changes in viscosity, and solution flow dynamics. They also provide a straightforward means and correct for nonspecific adsorption and nonspecific chemical reactions that may occur on or within the chemically selective coating. In addition, multiple targets can be detected simultaneously, leading to high-throughput measurements and producing distinct recognition patterns from complex mixtures.[139] We recommend that all future work with microcantilever sensor technology be performed using cantilever arrays.

The field of microcantilever sensors has matured to the point where reports of new applications of this technology should include performance testing under relevant conditions with measures of the fidelity and selectivity of detection. For example, if a new chemically selective cantilever coating is developed that provides a means for detecting a volatile analyte in air, then the report should include the performance of this coating when exposed to a variety of air samples (e.g., compressed air, laboratory air, auto exhaust, etc.). Similarly, reports of new biological applications should include results of tests carried out in the fluids where the analyte is typically found (e.g., sputum, serum, urine, and cell lysate). While there is some value to disseminating results of analyses carried out with pristine solutions, reports of successful detection of specific analytes in complex mixtures signifi-

cantly advances the field and provides strong impetus for increased commercial participation in the development of this sensor technology.

8.3. Fruitful Areas for Further Research

To become competitive with existing commercial sensing technologies (e.g., quartz crystal microbalance, surface plasmon resonance, and surface acoustic wave), microcantilever sensors must provide faster, cheaper, more sensitive, rugged, and reliable analyses. In addition, the microcantilever sensing system must be easy to operate and field deployable. On the basis of these benchmarks and the present state-of-the-art, there is a need for more research in the following areas.

8.3.1. More Selective Coatings

The quartz crystal microbalance and surface acoustic wave device are two commercialized sensing technologies that rely on changes in mass for detection. To compete with these technologies, analyses based on shifts in cantilever resonance either should be performed on short, stiff cantilevers with resonance frequencies in the MHz range, or by tracking shifts in one of the higher resonance modes of conventional cantilevers. The latter is preferred as the small dimensions of short, stiff cantilevers reduce the capacity of the sensor and, thus, the dynamic range of detection. We suggest increased effort in the development of new, highly selective coatings that give rise to large changes in surface stress upon analyte binding. It seems likely that these coatings will utilize highly specific biomolecular interactions. Also needed are novel packaging approaches to increase the shelf life of existing biomolecular coatings.

8.3.2. Increased Sensitivity and Faster Response

To compete favorably with benchmark sensing technologies, the speed and sensitivity of analysis with microcantilever sensors must be improved. Shortening the temporal response of cantilevers to analyte passing over the selective layer requires additional insight into the analyte-binding mechanism(s) as well as a dramatic reduction in the volume of the compartment in which the cantilever array is housed. The latter will require careful attention to the mass transport of analyte to the sensor surface and modeling of the fluid dynamics of analyte flow through the compartment and about the cantilevers. Thus, incorporation of arrays in microfluidics cartridges would seemingly be one way to shorten the response time.

Another approach is being pursued by the Manalis group at MIT.[224−226] They have achieved significantly enhanced sensitivity and very low limits of detection for fluidborne analytes using specially designed cantilevers that have integrated microfluidic channels within them (see Figure 15). The analyses are performed using optical lever detection with the cantilever under vacuum and sample flowing through the interior of the cantilever. This approach eliminates both the damping normally encountered when the cantilever is immersed in fluid and light scattering or absorption by the fluid sample, which negatively impacts optical lever detection. Selectivity in detection is achieved by precoating the walls of the microfluidics channel.[225] This very recent advance suggests that the present shortcomings which impede many applications of microcantilever technology will be removed through innovations in the design of cantilevers,

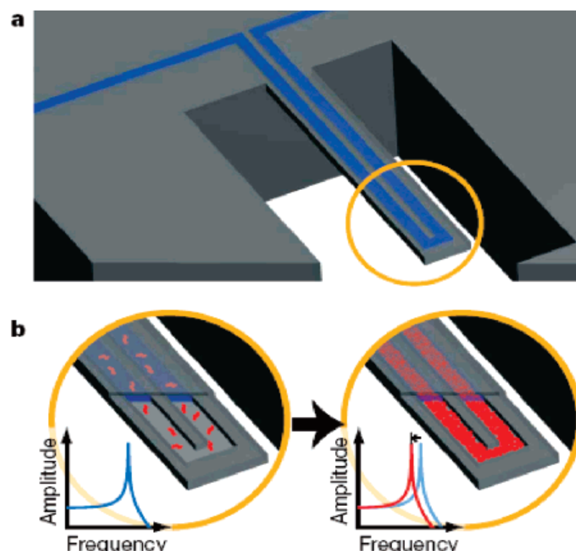

Figure 15. Schematic illustration of cantilevers with integrated microchannels developed by Manalis and co-workers. (a) A suspended microchannel translates mass changes into changes in resonance frequency. Fluid continuously flows through the channel and delivers biomolecules, cells, or synthetic particles. (b) While bound and unbound molecules both increase the mass of the channel, species that bind to the channel wall accumulate inside the device, and, as a result, their number can greatly exceed the number of free molecules in solution. This enables specific detection by way of immobilized receptors. Reprinted with permission from Burg et al. *Nature* **2007**, *446*, 1066. Copyright 2007 Nature Publishing Group.

detection devices, and sample delivery systems; intelligent design of coating-layer composition and high-throughput methods for their application; and incorporation of chemometric methods of analysis for processing data acquired with cantilever arrays. With more advances such as these, microcantilever technology will enable rapid detection of harmful agents that may be present in the air we breathe and the fluids we ingest.

9. References

(1) Gimzewski, J. K.; Gerber, C. H.; Mayer, E.; Schlitter, R. R. *Chem. Phys. Lett.* **1994**, *217*, 589.
(2) Gimzewski, J. K.; Gerber, C.; Meyer, E.; Schlittler, R. R. *NATO ASI Ser., Ser. E: Appl. Sci.* **1995**, *286*, 123.
(3) Chen, G. Y.; Thundat, T.; Wachter, E. A.; Warmack, R. J. *J. Appl. Phys.* **1995**, *77*, 3618.
(4) Thundat, T.; Chen, G. Y.; Warmack, R. J.; Allison, D. P.; Wachter, E. A. *Anal. Chem.* **1995**, *67*, 519.
(5) Thundat, T.; Wachter, E. A.; Sharp, S. L.; Warmack, R. J. *Appl. Phys. Lett.* **1995**, *66*, 1695.
(6) Wachter, E. A.; Thundat, T. *Rev. Sci. Instrum.* **1995**, *66*, 3662.
(7) McFarland, A. W.; Poggi, M. A.; Bottomley, L. A.; Colton, J. S. *J. Micromech. Microeng.* **2005**, *15*, 785.
(8) Then, D.; Vidic, A.; Ziegler, C. *Sens. Actuators, B* **2006**, *B117*, 1.
(9) Then, D.; Ziegler, C. *Encycl. Nanosci. Nanotechnol.* **2004**, *1*, 499.
(10) Abadal, G.; Davis, Z. J.; Helbo, B.; Borrise, X.; Ruiz, R.; Boisen, A.; Campabadal, F.; Esteve, J.; Figueras, E.; Perez-Murano, F.; Barniol, N. *Nanotechnology* **2001**, *12*, 100.
(11) Lang, H. P.; Berger, R.; Battiston, F.; Ramseyer, J. P.; Meyer, E.; Andreoli, C.; Brugger, J.; Vettiger, P.; Despont, M.; Mezzacasa, T.; Scandella, L.; Guentherodt, H. J.; Gerber, C.; Gimzewski, J. K. *Appl. Phys. A* **1998**, *66*, S61.
(12) Rasmussen, P. A.; Grigorov, A. V.; Boisen, A. *J. Micromech. Microeng.* **2005**, *15*, 1088.
(13) Lu, P.; Lee, H. P.; Lu, C.; O'Shea, S. J. *Phys. Rev. B: Condens. Matter* **2005**, *72*, 085405/1.
(14) Crandall, S. H.; Dahl, N. C. *An Introduction to the Mechanics of Solids*; McGraw-Hill, Inc.: New York, 1972.
(15) McFarland, A. W.; Poggi, M. A.; Bottomley, L. A.; Colton, J. S. *Nanotechnology* **2004**, *15*, 1628.

(16) Poggi, M. A.; McFarland, A. W.; Colton, J. S.; Bottomley, L. A. *Anal. Chem.* **2005**, *77*, 1192.
(17) Stoney, G. G. *Proc. R. Soc. London, Ser. A* **1909**, *82*, 172.
(18) McFarland, A. W.; Colton, J. S. *J. Micromech. Microeng.* **2005**, *15*, 1060.
(19) Sader, J. E. *J. Appl. Phys.* **2001**, *89*, 2911.
(20) McFarland, A. W. Ph.D. thesis, Georgia Institute of Technology, Atlanta, GA, 2005.
(21) Ginsberg, J. *Mechanical Structural Vibrations*; John Wiley and Sons: New York, 2001.
(22) Petersen, K. E.; Guarnieri, C. R. *J. Appl. Phys.* **1979**, *50*, 6761.
(23) Sandberg, R.; Moelhave, K.; Boisen, A.; Svendsen, W. *J. Micromech. Microeng.* **2005**, *15*, 2249.
(24) Tamayo, J. *J. Appl. Phys.* **2005**, *97*, 044903/1.
(25) Blom, F. R.; Bouwstra, S.; Elwenspoek, M.; Fluitman, J. H. J. *J. Vac. Sci. Technol., B* **1992**, *10*, 19.
(26) Fadel, L.; Dufour, I.; Lochon, F.; Francais, O. *Sens. Actuators, B* **2004**, *102*, 73.
(27) Tamayo, J.; Humphris, A. D. L.; Owen, R. J.; Miles, M. J. *Biophys. J.* **2001**, *81*, 526.
(28) Yasumura, K. Y.; Stowe, T. D.; Chow, E. M.; Pfafman, T.; Kenny, T. W.; Stipe, B. C.; Rugar, D. *J. Microelectromech. Syst.* **2000**, *9*, 117.
(29) Yang, J.; Ono, T.; Esashi, M. *Sens. Actuators, A* **2000**, *A82*, 102.
(30) Lei, F. H.; Nicolas, J. L.; Troyon, M.; Sockalingum, G. D.; Rubin, S.; Manfait, M. *J. Appl. Phys.* **2003**, *93*, 2236.
(31) McFarland, A. W.; Poggi, M. A.; Doyle, M. J.; Bottomley, L. A.; Colton, J. S. *Appl. Phys. Lett.* **2005**, *87*, 053505.
(32) Searle, G. F. C. *Experimental elasticity, a manual for the laboratory*; University Press: Cambridge, U.K., 1920.
(33) Kaldor, S. K.; Noyan, I. C. *Appl. Phys. Lett.* **2002**, *80*, 2284.
(34) Timoshenko, S. *Vibration Problems in Engineering*, fourth ed.; Wiley: New York, 1974.
(35) Timoshenko, S. P.; Goodier, J. N. *Theory of Elasticity*; McGraw-Hill, Inc.: New York, 1970.
(36) Han, S.; Benaroya, H.; Wei, T. *J. Sound Vib.* **1999**, *225*, 935.
(37) McFarland, A. W.; Colton, J. S. *J. Microelectromech. Syst.* **2005**, *14*, 1375.
(38) Sader, J. E. *J. Appl. Phys.* **1998**, *84*, 64.
(39) Sader, J. E.; Larson, I.; Mulvaney, P.; White, L. R. *Rev. Sci. Instrum.* **1995**, *66*, 3789.
(40) Lindholm, U. S.; Kana, D. D.; Chu, W.-H.; Abramson, H. N. *J. Ship Res.* **1965**, *9*, 11.
(41) Newell, W. E. *Science* **1968**, *161*, 1320.
(42) Battiston, F. M.; Ramseyer, J. P.; Lang, H. P.; Baller, M. K.; Gerber, C.; Gimzewski, J. K.; Meyer, E.; Guntherodt, H. J. *Sens. Actuators, B* **2001**, *B77*, 122.
(43) Wachtman, J. B., Jr.; Tefft, W. E.; Lam, D. G. J.; Apstein, C. S. *Phys. Rev. B* **1961**, *122*, 1754.
(44) Gysin, U.; Rast, S.; Ruff, P.; Meyer, E.; Lee, D. W.; Vettiger, P.; Gerber, C. *Phys. Rev. B: Condens. Matter* **2004**, *69*, 045403.
(45) Shekhawat, G.; Tark, S. H.; Dravid, V. P. *Science* **2006**, *311*, 1592.
(46) Bottomley, L. A.; Poggi, M. A.; Shen, S. X. *Anal. Chem.* **2004**, *76*, 5685.
(47) Alvarez, M.; Tamayo, J. *Sens. Actuators, B* **2005**, *B106*, 687.
(48) Mertens, J.; Alvarez, M.; Tamayo, J. *Appl. Phys. Lett.* **2005**, *87*, 234102/1.
(49) Baller, M. K.; Lang, H. P.; Fritz, J.; Gerber, C.; Gimzewski, J. K.; Drechsler, U.; Rothuizen, H.; Despont, M.; Vettiger, P.; Battiston, F. M.; Ramseyer, J. P.; Fornaro, P.; Meyer, E.; Guntherodt, H. J. *Ultramicroscopy* **2000**, *82*, 1.
(50) Lang, H. P.; Berger, R.; Andreoli, C.; Brugger, J.; Despont, M.; Vettiger, P.; Gerber, C.; Gimzewski, J. K.; Ramseyer, J. P.; Meyer, E.; Guntherodt, H. J. *Appl. Phys. Lett.* **1998**, *72*, 383.
(51) Arntz, Y.; Seelig, J. D.; Lang, H. P.; Zhang, J.; Hunziker, P.; Ramseyer, J. P.; Meyer, E.; Hegner, M.; Gerber, C. *Nanotechnology* **2003**, *14*, 86.
(52) Archibald, R.; Datskos, P.; Devault, G.; Lamberti, V.; Lavrik, N.; Noid, D.; Sepaniak, M.; Dutta, P. *Anal. Chim. Acta* **2007**, *584*, 101.
(53) Backmann, N.; Zahnd, C.; Huber, F.; Bietsch, A.; Pluckthun, A.; Lang, H. P.; Guntherodt, H. J.; Hegner, M.; Gerber, C. *Proc. Natl. Acad. Sci. U.S.A.* **2005**, *102*, 14587.
(54) Huber, F.; Hegner, M.; Gerber, C.; Guntherodt, H. J.; Lang, H. P. *Biosens. Bioelectron.* **2006**, *21*, 1599.
(55) Carrascosa, L. G.; Moreno, M.; Alvarez, M.; Lechuga, L. M. *TrAC Trends Anal. Chem.* **2006**, *25*, 196.
(56) Jeon, S.; Thundat, T. *Appl. Phys. Lett.* **2004**, *85*, 1083.
(57) Lim, S. H.; Raorane, D.; Satyanarayana, S.; Majumdar, A. *Sens. Actuators, B* **2006**, *119*, 466.
(58) Yue, M.; Lin, H.; Dedrick, D. E.; Satyanarayana, S.; Majumdar, A.; Bedekar, A. S.; Jenkins, J. W.; Sundaram, S. *J. Microelectromech. Syst.* **2004**, *13*, 290.
(59) Helm, M.; Servant, J. J.; Saurenbach, F.; Berger, R. *Appl. Phys. Lett.* **2005**, *87*, 064101/1.
(60) Raiteri, R.; Grattarola, M.; Butt, H. J.; Skladal, P. *Sens. Actuators, B* **2001**, *B79*, 115.
(61) Nieva, P. M.; McGruer, N. E.; Adams, G. G. *J. Micromech. Microeng.* **2006**, *16*, 2618.
(62) Reed, J.; Wilkinson, P.; Schmit, J.; Klug, W.; Gimzewski, J. K. *Nanotechnology* **2006**, *17*, 3873.
(63) Linnemann, R.; Gotszalk, T.; Hadjiiski, L.; Rangelow, I. W. *Thin Solid Films* **1995**, *264*, 159.
(64) Linnemann, R.; Gotszalk, T.; Rangelow, I. W.; Dumania, P.; Oesterschulze, E. *J. Vac. Sci. Technol., B* **1996**, *14*, 856.
(65) Britton, C. L.; Jones, R. L.; Oden, P. I.; Hu, Z.; Warmack, R. J.; Smith, S. F.; Bryan, W. L.; Rochelle, J. M. *Ultramicroscopy* **2000**, *82*, 17.
(66) Forsen, E.; Abadal, G.; Ghatnekar-Nilsson, S.; Teva, J.; Verd, J.; Sandberg, R.; Svendsen, W.; Perez-Murano, F.; Esteve, J.; Figueras, E.; Campabadal, F.; Montelius, L.; Barniol, N.; Boisen, A. *Appl. Phys. Lett.* **2005**, *87*.
(67) Amirola, J.; Rodriguez, A.; Castaner, L. *Proc. SPIE−Int. Soc. Opt. Eng.* **2003**, *5116*, 92.
(68) Amirola, J.; Rodriguez, A.; Castaner, L.; Santos, J. P.; Gutierrez, J.; Horrillo, M. C. *Sens. Actuators, B* **2005**, *B111−B112*, 247.
(69) Verd, J.; Abadal, G.; Teva, J.; Gaudo, M. V.; Uranga, A.; Borrise, X.; Campabadal, F.; Esteve, J.; Costa, E. F.; Perez-Murano, F.; Davis, Z. J.; Forsen, E.; Boisen, A.; Barniol, N. *J. Microelectromech. Syst.* **2005**, *14*, 508.
(70) Chatzandroulis, S.; Tserepi, A.; Goustouridis, D.; Normand, P.; Tsoukalas, D. *Microelectron. Eng.* **2002**, *61−62*, 955.
(71) Mertens, J.; Finot, E.; Thundat, T.; Fabre, A.; Nadal, M. H.; Eyraud, V.; Bourillot, E. *Ultramicroscopy* **2003**, *97*, 119.
(72) Plaza, J. A.; Zinoviev, K.; Villanueva, G.; Alvarez, M.; Tamayo, J.; Dominguez, C.; Lechuga, L. M. *Appl. Phys. Lett.* **2006**, *89*, 094109/1.
(73) Hierlemann, A.; Brand, O.; Hagleitner, C.; Baltes, H. *Proc. IEEE* **2003**, *91*, 839.
(74) Madou, M. *Fundamentals of Microfabrication: The Science of Miniaturization*, second ed.; CRC Press: Boca Raton, FL, 2002.
(75) Jastrzebski, L.; Corboy, J. F.; Soydan, R. *J. Electrochem. Soc.* **1989**, *136*, 3506.
(76) Jastrzebski, L.; Corboy, J. F.; McGinn, J. T.; Pagliaro, R., Jr. *J. Electrochem. Soc.* **1983**, *130*, 1571.
(77) Jenkins, N. E.; DeFlores, L. P.; Allen, J.; Ng, T. N.; Garner, S. R.; Kuehn, S.; Dawlaty, J. M.; Marohn, J. A. *J. Vac. Sci. Technol., B* **2004**, *22*, 909.
(78) Minne, S. C.; Manalis, S. R.; Quate, C. F. *Bringing Scanning Probe Microscopy Up to Speed*; Kluwer: Boston, MA, 1999.
(79) Nesterov, V.; Brand, U. *J. Micromech. Microeng.* **2006**, *16*, 1116.
(80) Okamoto, H.; Akazaki, T.; Ueki, M.; Yamaguchi, H.; Namatsu, H. *Physica E* **2006**, *32*, 512.
(81) Yu, X. M.; Thaysen, J.; Hansen, O.; Boisen, A. *J. Appl. Phys.* **2002**, *92*, 6296.
(82) Zuo, G.; Li, X.; Li, P.; Yang, T.; Wang, Y.; Cheng, Z.; Feng, S. *Anal. Chim. Acta* **2006**, *580*, 123.
(83) Campbell, G. A.; Mutharasan, R. *Biosens. Bioelectron.* **2006**, *22*, 35.
(84) Campbell, G. A.; Mutharasan, R. *Anal. Chem.* **2006**, *78*, 2328.
(85) Shih, W. Y.; Li, X. P.; Gu, H. M.; Shih, W. H.; Aksay, I. A. *J. Appl. Phys.* **2001**, *89*, 1497.
(86) Detzel, A. J.; Campbell, G. A.; Mutharasan, R. *Sens. Actuators, B* **2006**, *B117*, 58.
(87) Yi, J. W.; Shih, W. Y.; Mutharasan, R.; Shih, W.-H. *J. Appl. Phys.* **2003**, *93*, 619.
(88) Yi, J. W.; Shih, W. Y.; Shih, W. H. *J. Appl. Phys.* **2002**, *91*, 1680.
(89) Lee, Y.; Lim, G.; Moon, W. *Sens. Actuators, A* **2006**, *A130−A131*, 105.
(90) Mortet, V.; Haenen, K.; Potmesil, J.; Vanecek, M.; D'Olieslaeger, M. *Phys. Status Solidi A* **2006**, *203*, 3185.
(91) Davis, Z. J.; Abadal, G.; Helbo, B.; Hansen, O.; Campabadal, F.; Perez-Murano, F.; Esteve, J.; Figueras, E.; Verd, J.; Barniol, N.; Boisen, A. *Sens. Actuators, A* **2003**, *A105*, 311.
(92) Forsen, E.; Nilsson, S. G.; Carlberg, P.; Abadal, G.; Perez-Murano, F.; Esteve, J.; Montserrat, J.; Figueras, E.; Campabadal, F.; Verd, J.; Montelius, L.; Barniol, N.; Boisen, A. *Nanotechnology* **2004**, *15*, S628.
(93) Jenkins, D. F. L.; Clegg, W. W.; Cattan, E.; Remiens, D. *J. Electroceram.* **2001**, *7*, 5.
(94) Jiguet, S.; Bertsch, A.; Hofmann, H.; Renaud, P. *Adv. Eng. Mater.* **2004**, *6*, 719.
(95) Curran, S.; Ajayan, P. M.; Blau, W.; Carroll, D. L.; Coleman, J. N.; Dalton, A.; Davey, A. P.; McCarthy, B. *Adv. Mater.* **1998**, *10*, 1091.
(96) Calleja, M.; Nordstroem, M.; Alvarez, M.; Tamayo, J.; Lechuga, L. M.; Boisen, A. *Ultramicroscopy* **2005**, *105*, 215.

(97) Calleja, M.; Tamayo, J.; Nordstrom, M.; Boisen, A. *Appl. Phys. Lett.* **2006**, *88*.
(98) Ransley, J. H. T.; Watari, M.; Sukumaran, D.; McKendry, R. A.; Seshia, A. A. *Microelectron. Eng.* **2006**, *83*, 1621.
(99) Johansson, A.; Calleja, M.; Rasmussen, P. A.; Boisen, A. *Sens. Actuators, A* **2005**, *A123*−*A124*, 111.
(100) Johansson, A.; Blagoi, G.; Boisen, A. *Appl. Phys. Lett.* **2006**, *89*, 173505.
(101) McFarland, A. W.; Poggi, M. A.; Bottomley, L. A.; Colton, J. S. *Nanotechnology* **2005**, *16*, 1249.
(102) Hu, Z.; Thundat, T.; Warmack, R. J. *Proc. Electrochem. Soc.* **1999**, *99*−*23*, 347.
(103) Rogers, B.; Bauer, C. A.; Adams, J. D. *MEM Syst.* **2003**, *5*, 663.
(104) Rogers, B.; Manning, L.; Jones, M.; Sulchek, T.; Murray, K.; Beneschott, B.; Adams, J. D.; Hu, Z.; Thundat, T.; Cavazos, H.; Minne, S. C. *Rev. Sci. Instrum.* **2003**, *74*, 4899.
(105) Chang, C. P.; Wang, Y. S.; Huang, R. S. *Jpn. J. Appl. Phys., Part 1* **2004**, *43*, 5491.
(106) Leichle, T.; Silvan, M. M.; Belaubre, P.; Valsesia, A.; Ceccone, G.; Rossi, F.; Saya, D.; Pourciel, J.-B.; Nicu, L.; Bergaud, C. *Nanotechnology* **2005**, *16*, 525.
(107) Fagan, B. C.; Tipple, C. A.; Xue, Z. L.; Sepaniak, M. J.; Datskos, P. G. *Talanta* **2000**, *53*, 599.
(108) Dutta, P.; Senesac, L. R.; Lavrik, N. V.; Datskos, P. G.; Sepaniak, M. J. *Sens. Lett.* **2004**, *2*, 238.
(109) Headrick, J. J.; Sepaniak, M. J.; Lavrik, N. V.; Datskos, P. G. *Ultramicroscopy* **2003**, *97*, 417.
(110) Tipple, C. A.; Lavrik, N. V.; Culha, M.; Headrick, J.; Datskos, P.; Sepaniak, M. J. *Anal. Chem.* **2002**, *74*, 3118.
(111) Lavrik, N. V.; Tipple, C. A.; Datskos, P. G.; Sepaniak, M. J. *Proc. SPIE*−*Int. Soc. Opt. Eng.* **2001**, *4560*, 152.
(112) Hilt, J. Z.; Gupta, A. K.; Bashir, R.; Peppas, N. A. *Mater. Res. Soc. Symp. Proc.* **2002**, *729*, 173.
(113) Bashir, R.; Hilt, J. Z.; Elibol, O.; Gupta, A.; Peppas, N. A. *Appl. Phys. Lett.* **2002**, *81*, 3091.
(114) Hilt, J. Z.; Gupta, A. K.; Bashir, R.; Peppas, N. A. *Biomed. Microdev.* **2003**, *5*, 177.
(115) Zhang, Y.; Ji, H.-F.; Snow, D.; Sterling, R.; Brown, G. M. *Instrum. Sci. Technol.* **2004**, *32*, 361.
(116) Liu, K.; Ji, H. F. *Anal. Sci.* **2004**, *20*, 9.
(117) Zhang, Y. F.; Ji, H. F.; Brown, G. M.; Thundat, T. *Anal. Chem.* **2003**, *75*, 4773.
(118) Zhang, Y. F.; Ji, H. F.; Snow, D.; Sterling, R.; Brown, G. M. *Instrum. Sci. Technol.* **2004**, *32*, 361.
(119) Betts, T. A.; Tipple, C. A.; Sepaniak, M. J.; Datskos, P. G. *Anal. Chim. Acta* **2000**, *422*, 89.
(120) Sayer, M.; Barrow, D.; Zou, L.; Kumar, C. V. R. V.; Noteboom, R.; Knapik, D. A.; Schindel, D. W.; Hutchins, D. A. *Mater. Res. Soc. Symp. Proc.* **1993**, *310*, 37.
(121) Chapman, P. J.; Vogt, F.; Dutta, P.; Datskos, P. G.; Devault, G. L.; Sepaniak, M. J. *Anal. Chem.* **2007**, *79*, 364.
(122) Senesac, L. R.; Dutta, P.; Datskos, P. G.; Sepaniak, M. J. *Anal. Chim. Acta* **2006**, *558*, 94.
(123) Dutta, P.; Chapman, P. J.; Datskos, P. G.; Sepaniak, M. J. *Anal. Chem.* **2005**, *77*, 6601.
(124) Porter, T. L.; Eastman, M. P.; Pace, D. L.; Bradley, M. *Sens. Actuators, A* **2001**, *A88*, 47.
(125) Fritz, J.; Baller, M. K.; Lang, H. P.; Rothuizen, H. V. P.; Meyer, E.; Guntherodt, H.-J.; Gerber, C.; Gimzewski, J. K. *Science* **2000**, *288*, 316.
(126) Zhang, J.; Lang, H. P.; Huber, F.; Bietsch, A.; Grange, W.; Certa, U.; McKendry, R.; Guntherodt, H. J.; Hegner, M.; Gerber, C. *Nature Nanotechnol.* **2006**, *1*, 214.
(127) McKendry, R.; Zhang, J.; Arntz, Y.; Strunz, T.; Hegner, M.; Lang, H. P.; Baller, M. K.; Certa, U.; Meyer, E.; Guntherodt, H.-J.; Gerber, C. *Proc. Natl. Acad. Sci. U.S.A.* **2002**, *99*, 9783.
(128) Mukhopadhyay, R.; Lorentzen, M.; Kjems, J.; Besenbacher, F. *Langmuir* **2005**, *21*, 8400.
(129) Bietsch, A.; Zhang, J. Y.; Hegner, M.; Lang, H. P.; Gerber, C. *Nanotechnology* **2004**, *15*, 873.
(130) Dhayal, B.; Henne, W. A.; Doorneweerd, D. D.; Reifenberger, R. G.; Low, P. S. *J. Am. Chem. Soc.* **2006**, *128*, 3716.
(131) Belaubre, P.; Guirardel, M.; Garcia, G.; Pourciel, J. B.; Leberre, V.; Dagkessamanskaia, A.; Trevisiol, E.; Francois, J. M.; Bergaud, C. *Appl. Phys. Lett.* **2003**, *82*, 3122.
(132) Wu, S.-Y.; Berkenbosch, R.; Lui, A.; Green, J.-B. D. *Analyst (Cambridge, U. K.)* **2006**, *131*, 1213.
(133) Zou, J.; Bullen, D.; Wang, X.; Liu, C.; Mirkin, C. A. *Appl. Phys. Lett.* **2003**, *83*, 581.
(134) Banerjee, D. *BioMEMS Biomed. Nanotechnol.* **2006**, *1*, 265.
(135) Chisholm, R. A.; Qiu, W.; Green, J.-B. D. *Langmuir* **2007**, *23*, 7891.
(136) Green, J.-B. D. *Anal. Chim. Acta* **2003**, *496*, 267.
(137) Thundat, T.; Oden, P. I.; Warmack, R. J. *Microscale Thermophys. Eng.* **1997**, *1*, 185.
(138) Thundat, T.; Oden, P. I.; Warmack, R. J. *Proc. Electrochem. Soc.* **1997**, *97*−*5*, 179.
(139) Lang, H. P.; Hegner, M.; Meyer, E.; Gerber, C. *Nanotechnology* **2002**, *13*, R29.
(140) Raiteri, R.; Grattarola, M.; Berger, R. *Materials Today (Oxford, U. K.)* **2002**, *5*, 22.
(141) Datskos, P. G.; Lavrik, N. V.; Sepaniak, M. J. *NATO Sci. Ser., II* **2004**, *181*, 331.
(142) Datskos, P. G.; Lavrik, N. V.; Sepaniak, M. J. *Intro. Nanoscale Sci. Technol.* **2004**, 417.
(143) Datskos, P. G.; Thundat, T.; Lavrik, N. V. *Encycl. Nanosci. Nanotechnol.* **2004**, *5*, 551.
(144) Lavrik, N. V.; Sepaniak, M. J.; Datskos, P. G. *Rev. Sci. Instrum.* **2004**, *75*, 2229.
(145) Lang, H. P.; Baller, M. K.; Berger, R.; Gerber, C.; Gimzewski, J. K.; Battiston, F. M.; Fornaro, P.; Ramseyer, J. P.; Meyer, E.; Guntherodt, H. J. *Anal. Chim. Acta* **1999**, *393*, 59.
(146) Maute, M.; Raible, S.; Prins, F. E.; Kern, D. P.; Ulmer, H.; Weimar, U.; Gopel, W. *Sens. Actuators, B* **1999**, *B58*, 505.
(147) Maute, M.; Raible, S.; Prins, F. E.; Kern, D. P.; Weimar, U.; Gopel, W. *Microelectron. Eng.* **1999**, *46*, 439.
(148) Kim, B. H.; Maute, M.; Prins, F. E.; Kern, D. P.; Croitoru, M.; Raible, S.; Weimar, U.; Gopel, W. *Microelectron. Eng.* **2000**, *53*, 229.
(149) Kim, B. H.; Prins, F. E.; Kem, D. P.; Raible, S.; Weimar, U. *Sens. Actuators, B* **2001**, *78*, 12.
(150) Lange, D.; Hagleitner, C.; Hierlemann, A.; Brand, O.; Baltes, H. *Anal. Chem.* **2002**, *74*, 3084.
(151) Kurzawski, P.; Hagleitner, C.; Hierlemann, A. *Anal. Chem.* **2006**, *78*, 6910.
(152) Fadel, L.; Lochon, F.; Dufour, I.; Francais, O. *J. Micromech. Microeng.* **2004**, *14*, S23.
(153) Vidic, A.; Then, D.; Ziegler, C. *Ultramicroscopy* **2003**, *97*, 407.
(154) Lechuga, L. M.; Tamayo, J.; Calle, A.; Calleja, M.; Dominquez, C. *NATO Sec. Sci. Ser., Ser. B* **2005**, *1*, 175.
(155) Pinnaduwage, L. A.; Gehl, A.; Hedden, D. L.; Muralidharan, G.; Thundat, T.; Lareau, R. T.; Sulchek, T.; Manning, L.; Rogers, B.; Jones, M.; Adams, J. D. *Nature (London, U. K.)* **2003**, *425*, 474.
(156) Pinnaduwage, L. A.; Ji, H.-F.; Thundat, T. *IEEE Sens. J.* **2005**, *5*, 774.
(157) Pinnaduwage, L. A.; Wig, A.; Hedden, D. L.; Gehl, A.; Yi, D.; Thundat, T.; Lareau, R. T. *J. Appl. Phys.* **2004**, *95*, 5871.
(158) Ji, H. F.; Yan, X.; Lu, Y.; Du, H.; Thundat, T. *Proc. SPIE*−*Int. Soc. Opt. Eng.* **2006**, *6223*, 622307/1.
(159) Ji, H. F.; Yan, X. D.; Zhang, J.; Thundat, T. *Expert Rev. Mol. Diagn.* **2004**, *4*, 859.
(160) Pinnaduwage, L. A.; Gehl, A. C.; Allman, S. L.; Johansson, A.; Boisen, A. *Rev. Sci. Instrum.* **2007**, *78*, 055101.
(161) Voiculescu, I.; Zaghloul, M. E.; McGill, R. A.; Houser, E. J.; Fedder, G. K. *IEEE Sens. J.* **2005**, *5*, 641.
(162) Voiculescu, I. R.; Zaghloul, M. E.; McGill, R. A.; Vignola, J. F. *Proc. Inst. Mech. Eng., Part C* **2006**, *220*, 1601.
(163) Zuo, G. M.; Li, X. X.; Li, P.; Yang, T. T.; Wang, Y. L.; Cheng, Z. X.; Feng, S. L. *Anal. Chim. Acta* **2006**, *580*, 123.
(164) Yang, Y.; Ji, H.-F.; Thundat, T. *J. Am. Chem. Soc.* **2003**, *125*, 1124.
(165) Karnati, C.; Dua, H.; Ji, H.-F.; Xua, X.; Lvov, Y.; Mulchandani, A.; Mulchandani, P.; Chen, W. *Biosens. Bioelectron.* **2007**, *22*, 2636.
(166) Pamula, V. K.; Fair, R. B. *Proc. SPIE*−*Int. Soc. Opt. Eng.* **1999**, *3710*, 321.
(167) Pamula, V. K.; Fair, R. B. *Proc. SPIE*−*Int. Soc. Opt. Eng.* **2000**, *4038*, 547.
(168) Thundat, T.; Pinnaduwage, L.; Lareau, R. *NATO Sci. Ser., II* **2004**, *159*, 249.
(169) Rogers, B.; Whitten, R.; Adams, J. D. *Proc. SPIE*−*Int. Soc. Opt. Eng.* **2006**, *6201*, 62010G/1.
(170) Rogers, B.; Whitten, R.; Adams, J. D. *Proc. SPIE*−*Int. Soc. Opt. Eng.* **2005**, *5986*, 59860O/1.
(171) Rogers, B.; Whitten, R.; Adams, J. D. *Proc. SPIE*−*Int. Soc. Opt. Eng.* **2006**, *6394*, 639409/1.
(172) Xu, X. H.; Thundat, T. G.; Brown, G. M.; Ji, H. F. *Anal. Chem.* **2002**, *74*, 3611.
(173) Ji, H.-F.; Thundat, T. *Biosens. Bioelectron.* **2002**, *17*, 337.
(174) Ji, H.-F.; Thundat, T.; Dabestani, R.; Brown, G. M.; Britt, P. F.; Bonnesen, P. V. *Anal. Chem.* **2001**, *73*, 1572.
(175) Ji, H.-F.; Finot, E.; Dabestani, R.; Brown, G. M.; Britt, P. F. *Chem. Commun. (Cambridge)* **2000**, 457.
(176) Ilic, B.; Czaplewski, D.; Craighead, H. G.; Neuzil, P.; Campagnolo, C.; Batt, C. *Appl. Phys. Lett.* **2000**, *77*, 450.
(177) Zhang, J.; Ji, H. F. *Anal. Sci.* **2004**, *20*, 585.
(178) Campbell, G. A.; Mutharasan, R. *Biosens. Bioelectron.* **2005**, *21*, 462.
(179) Campbell, G. A.; Mutharasan, R. *Anal. Sci.* **2005**, *21*, 355.

(180) Gfeller, K. Y.; Nugaeva, N.; Hegner, M. *Appl. Environ. Microbiol.* **2005**, *71*, 2626.
(181) Gfeller, K. Y.; Nugaeva, N.; Hegner, M. *Biosens. Bioelectron.* **2005**, *21*, 528.
(182) Ramos, D.; Tamayo, J.; Mertens, J.; Calleja, M.; Zaballos, A. *J. Appl. Phys.* **2006**, *100*.
(183) Ilic, B.; Yang, Y.; Craighead, H. G. *Appl. Phys. Lett.* **2004**, *85*, 2604.
(184) Gupta, A.; Akin, D.; Bashir, R. *Appl. Phys. Lett.* **2004**, *84*, 1976.
(185) Johnson, L.; Gupta, A. K.; Ghafoor, A.; Akin, D.; Bashir, R. *Sens. Actuators, B* **2006**, *B115*, 189.
(186) Campbell, G. A.; Mutharasan, R. *Biosens. Bioelectron.* **2006**, *22*, 78.
(187) Campbell, G. A.; Mutharasan, R. *Biosens. Bioelectron.* **2006**, *21*, 1684.
(188) Campbell, G. A.; Mutharasan, R. *Anal. Chem.* **2007**, *79*, 1145.
(189) Nugaeva, N.; Gfeller, K. Y.; Backmann, N.; Lang, H. P.; Dueggelin, M.; Hegner, M. *Biosens. Bioelectron.* **2005**, *21*, 849.
(190) Grogan, C.; Raiteri, R.; O'Connor, G. M.; Glynn, T. J.; Cunningham, V.; Kane, M.; Charlton, M.; Leech, D. *Biosens. Bioelectron.* **2002**, *17*, 201.
(191) Alvarez, M.; Calle, A.; Tamayo, J.; Lechuga, L. M.; Abad, A.; Montoya, A. *Biosens. Bioelectron.* **2003**, *18*, 649.
(192) Backmann, N.; Zahnd, C.; Huber, F.; Bietsch, A.; Pluckthun, A.; Lang, H.-P.; Guntherodt, H.-J.; Hegner, M.; Gerber, C. *Proc. Natl. Acad. Sci. U.S.A.* **2005**, *102*, 14587.
(193) Dutta, P.; Tipple, C. A.; Lavrik, N. V.; Datskos, P. G.; Hofstetter, H.; Hofstetter, O.; Sepaniak, M. J. *Anal. Chem.* **2003**, *75*, 2342.
(194) Hwang, K. S.; Lee, J. H.; Park, J.; Yoon, D. S.; Park, J. H.; Kim, T. S. *Lab Chip* **2004**, *4*, 547.
(195) Lee, J. H.; Hwang, K. S.; Park, J.; Yoon, K. H.; Yoon, D. S.; Kim, T. S. *Biosens. Bioelectron.* **2005**, *20*, 2157.
(196) Wee, K. W.; Kang, G. Y.; Park, J.; Kang, J. Y.; Yoon, D. S.; Park, J. H.; Kim, T. S. *Chem. Sens.* **2004**, *20*, 216.
(197) Wee, K. W.; Kang, G. Y.; Park, J.; Kang, J. Y.; Yoon, D. S.; Park, J. H.; Kim, T. S. *Biosens. Bioelectron.* **2005**, *20*, 1932.
(198) Lee, J. H.; Yoon, K. H.; Hwang, K. S.; Park, J.; Ahn, S.; Kim, T. S. *Biosens. Bioelectron.* **2004**, *20*, 269.
(199) Lee, J. H.; Kim, T. S.; Yoon, K. H. *Appl. Phys. Lett.* **2004**, *84*, 3187.
(200) Kang, G. Y.; Han, G. Y.; Kang, J. Y.; Cho, I.-H.; Park, H.-H.; Paek, S.-H.; Kim, T. S. *Sens. Actuators, B* **2006**, *B117*, 332.
(201) Wu, G.; Datar, R. H.; Hansen, K. M.; Thundat, T.; Cote, R. J.; Majumdar, A. *Nat. Biotechnol.* **2001**, *19*, 856.
(202) Hansen, K. M.; Ji, H. F.; Wu, G. H.; Datar, R.; Cote, R.; Majumdar, A.; Thundat, T. *Anal. Chem.* **2001**, *73*, 1567.
(203) Wu, G. H.; Ji, H. F.; Hansen, K. M.; Thundat, T.; Datar, R.; Cote, R.; Hagan, M. F.; Chakraborty, A. K.; Majumdar, A. *Proc. Natl. Acad. Sci. U.S.A.* **2001**, *98*, 1560.
(204) Hagan, M. F.; Majumdar, A.; Chakraborty, A. K. *J. Phys. Chem. B* **2002**, *106*, 10163.
(205) Alvarez, M.; Carrascosa, L. G.; Moreno, M.; Calle, A.; Zaballos, A.; Lechuga, L. M.; Martinez, A. C.; Tamayo, J. *Langmuir* **2004**, *20*, 9663.
(206) Stachowiak, J. C.; Yue, M.; Castelino, K.; Chakraborty, A.; Majumdar, A. *Langmuir* **2006**, *22*, 263.
(207) Biswal, S. L.; Raorane, D.; Chaiken, A.; Birecki, H.; Majumdar, A. *Anal. Chem.* **2006**, *78*, 7104.
(208) Biswal, S. L.; Raorane, D.; Chaiken, A.; Majumdar, A. *Jala* **2006**, *11*, 222.
(209) Marie, R.; Thaysen, J.; Christensen, C. B. V.; Boisen, A. *Spec. Publ.—R. Soc. Chem.* **2004**, *297*, 485.
(210) Gunter, R. L.; Zhine, R.; Delinger, W. G.; Manygoats, K.; Kooser, A.; Porter, T. L. *IEEE Sens. J.* **2004**, *4*, 430.
(211) Zhang, X. R.; Xu, X. F. *Appl. Phys. Lett.* **2004**, *85*, 2423.
(212) Su, M.; Li, S. U.; Dravid, V. P. *Appl. Phys. Lett.* **2003**, *82*, 3562.
(213) Subramanian, A.; Oden, P. I.; Kennel, S. J.; Jacobson, K. B.; Warmack, R. J.; Thundat, T.; Doktycz, M. J. *Appl. Phys. Lett.* **2002**, *81*, 385.
(214) Yan, X. D.; Ji, H. F.; Lvov, Y. *Chem. Phys. Lett.* **2004**, *396*, 34.
(215) Yan, X. D.; Xu, X. H. K.; Ji, H. F. *Anal. Chem.* **2005**, *77*, 6197.
(216) Pei, J. H.; Tian, F.; Thundat, T. *Anal. Chem.* **2004**, *76*, 292.
(217) Bottomley, L. A.; Ghosh, M.; Shen, S.; Saul, R.; Kossek, S.; Pace, G. W. U. S. Patent 7,141,385, 2006.
(218) Stevenson, K. A.; Mehta, A.; Sachenko, P.; Hansen, K. M.; Thundat, T. *Langmuir* **2002**, *18*, 8732.
(219) Liu, W.; Montana, V.; Chapman, E. R.; Mohideen, U.; Parpura, V. *Proc. Natl. Acad. Sci. U.S.A.* **2003**, *100*, 13621.
(220) Weizmann, Y.; Elnathan, R.; Lioubashevski, O.; Willner, I. *Nano Lett.* **2005**, *5*, 741.
(221) Weizmann, Y.; Elnathan, R.; Lioubashevski, O.; Willner, I. *J. Am. Chem. Soc.* **2005**, *127*, 12666.
(222) Barnes, J. R.; Stephenson, R. J.; Welland, M. E.; Gerber, C.; Gimzewski, J. K. *Nature* **1994**, *372*, 79.
(223) Barnes, J. R.; Stephenson, R. J.; Woodburn, C. N.; O'Shea, S. J.; Welland, M. E.; Rayment, T.; Gimzewski, J. K.; Gerber, C. *Rev. Sci. Instrum.* **1994**, *65*, 3793.
(224) Burg, T. P.; Godin, M.; Knudsen, S. M.; Shen, W.; Carlson, G.; Foster, J. S.; Babcock, K.; Manalis, S. R. *Nature* **2007**, *446*, 1066.
(225) Burg, T. P.; Manalis, S. R. *Appl. Phys. Lett.* **2003**, *83*, 2698.
(226) Burg, T. P.; Mirza, A. R.; Milovic, N.; Tsau, C. H.; Popescu, G. A.; Foster, J. S.; Manalis, S. R. *J. Microelectromech. Syst.* **2006**, *15*, 1466.

CR0681041